2013

Method for Determination of Kinematic Sensor Position and Orientation from Magnetic Resonance Images

Caglar Ozturk
Cleveland State University

METHOD FOR DETERMINATION OF KINEMATIC SENSOR POSITION AND ORIENTATION FROM MAGNETIC RESONANCE IMAGES

CAGLAR OZTURK

Bachelor of Science in Mechatronics Engineering

Bahcesehir University

July 2012

Submitted in partial fulfillment of requirements for the degree

MASTER OF SCIENCE IN BIOMEDICAL ENGINEERING

at the

CLEVELAND STATE UNIVERSITY

June 2013

This thesis has been approved

for the Department of CHEMICAL AND BIOMEDICAL ENGINEERING

and the College of Graduate Studies by

_____

Thesis Chairperson, Dr. Adam J. Bartsch

Spine Research Laboratory, Cleveland Clinic / 06.05.2013
Department & Date

_____

Dr. Nolan Holland

Chemical and Biomedical Engineering, Cleveland State University / 06.05.2013
Department & Date

_____

Dr. Sridhar Ungarala

Chemical and Biomedical Engineering, Cleveland State University / 06.05.2013
Department & Date

ACKNOWLEDGMENT

It is a pleasure to thank those who made this thesis possible. I would like to acknowledge the advice and guidance of my advisor, Dr. Adam Bartsch. He has been more than a mentor to me guiding me throughout my entire time. I sincerely thank him for introducing me to the research of Medical Image Processing. I also would like to thank Dr. Orhan Talu, Dr. Joanne Belovich, Dr.Majid Rashidi, Dr. Nolan Holland and Sergey Samorezov for playing a pivotal role in my thesis.

I sincerely acknowledge the support and encouragement of all of my friends and family members without which I wouldn't have been able to finish my degree. Moreover, I offer my regards and blessing to all of the people, especially Rebecca Laird and Darlene Montgomery, who did not hesitate to help me in my entire life in the US.

METHOD FOR DETERMINATION OF KINEMATIC SENSOR POSITION AND ORIENTATION FROM MAGNETIC RESONANCE IMAGES

CAGLAR OZTURK

ABSTRACT

Concussion and mild traumatic brain injury risk remain high for young athletes participating in helmeted and non-helmeted sports. Because of the short and potential long-term effects on young athletes and early onset Alzheimer's and Parkinson's disease, there is a dire need to correlate a relationship between head impact intensity, frequency, duration and athlete brain health. To address this need, the Cleveland Clinic is developing a custom mouthguard embedded with flexible circuitry and sensors, known as the "Intelligent Mouthguard"(IMG).

To accurately quantify peak values of head impacts or concussions, orientation and position of each sensor relative to CG (Center of Gravity) of human head should be calculated.

In this study, registration of IMG PCB sensor position and orientation from magnetic resonance images (MRI) was developed and implemented as an image processing method. This method consisted of creating both "Rigid MRI PCB" and "Human MRI PCB" from the same MRI visible material (Fullcure705) having exactly the same dimensions as the IMG PCB. As a Validation Part 1, the "Rigid MRI PCB" was scanned by itself and compared with a reference CAD drawing of the PCB called "CAD Image". In Validation Part 2, "Human MRI PCB" was scanned while inside a volunteer's mouth. Custom written MATLAB code was

used as an image post-processing tool in order to extract IMG PCB sensor position and orientation data with respect to the CG of the volunteer's head.

In summary, the method expresses a very simple but reliable and efficient way to obtain any position and orientation data with respect to a human subject's head anthropometry. The method gave **0.46 mm** maximum difference in position determination and **2.1°** difference as an angle for orientation. This means if an athlete received an impact which effects CG as **132.7g** impact in X direction, impact can be calculated **132.1g** or **133.6g** from Sensor 3 due to IMG position and orientation inaccuracies. Therefore, IMG measurement uncertainty is in the **±1%** range based on sensor position and orientation calculation. Future work should involve in vivo validation testing using more human scans and correlating external anthropometric landmarks with sensors' positions determined by MRI.

TABLE OF CONTENTS

LIST OF TABLES

LIST OF FIGURES

CHAPTER I

INTRODUCTION & BACKGROUND

The brain functions as the regulator center for all of the body's tasks. Brain injury may be the result of severe head trauma or a closed head injury and it can affect some or all of brain functions. Therefore, brain injury can lead to serious physical and mental effects. Loss of consciousness, paralysis, memory and personality problems can be given as an example for these effects.

A concussion is a serious type of traumatic brain injury. Even these injuries are described as “mild”, their effects can be serious. Traumatic brain injury (TBI) can be categorized into two types such as focal and diffuse brain injuries. If head contact occurs, it is described as focal brain injuries and they are the instant result of the trauma.

Diffuse brain injuries occur because of linear and rotational forces which emerges at the time of impact. These cause shearing or tensile stresses on the brain tissues. When the head impact occurs, those can lead human to going into

coma or stroke. These conditions have pointed out that there is a dire need to quantify the effect of an impact on the brain. [4].

In sports event such as football, hockey and boxing, there are 1.12 million mild TBI event happened [4]. In addition, according to the National Football Leagues (NFL) Injury Surveillance System from 1997 to 2002, 182 total head impacts were observed related TBI. The possible brain injury risk in European and American football has open research area about nature, mechanics and possible long-term effects of the practice. However, if these head injuries happen periodically, they can be fatal [5]. These problems have pointed out the necessary of monitoring the consequences of all head strikes on the human brain.

These necessities have led Cleveland Clinic to develop a mouth guard which can measure the impact of sports-related hits suffered by athletes on the field. It will measure the severity of brain injuries and can provide user-specific kinematics.

Figure 1. - Prototype of Intelligent Mouth Guard (IMG) Version 3.0 (v3.0)

As a concept, the IMG will be capable to quantify the peak and temporal values of different types of head impact or concussion. It measures both linear acceleration, in the unit of gravitational force (g), and angular velocity (rad/s), including the time interval (ms) of each head concussions. Angular acceleration (rad/s^2) and impact orientation can also be calculated.

IMG will measure head acceleration and rotation to relate to concussion injury risk. However, in order to calculate head center of gravity acceleration (a_{cg}) requires equations combining IMG measurements and landmarks on the head. Because human brain cannot be cut and sensors cannot be located into human brain. For this reason, measured data should be transformed to a_{cg} .

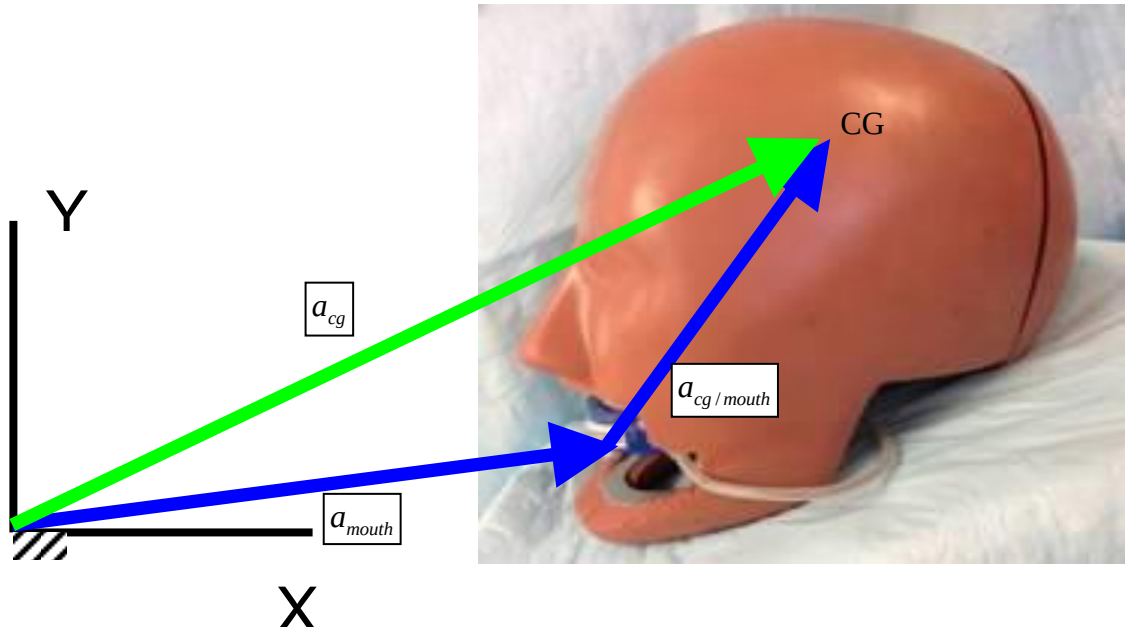

Figure 2. - a_{cg} and a_{mouth} transformation

$a_{cg} = a_{mouth} + a_{cg/mouth}$. a_{cg} cannot be directly measured in live human. Therefore a_{mouth} and $a_{cg/mouth}$ can be directly measured to calculate a_{cg} . a_{cg} requires unique transformation/algorithm combining IMG measurements and landmarks on the head. Transformation algorithm is based on Rigid Body Motion Equations. Rigid Body Equations will be used to transform a_{mouth} to a_{cg}.

A brief description is given below on general rigid body motion is written below:

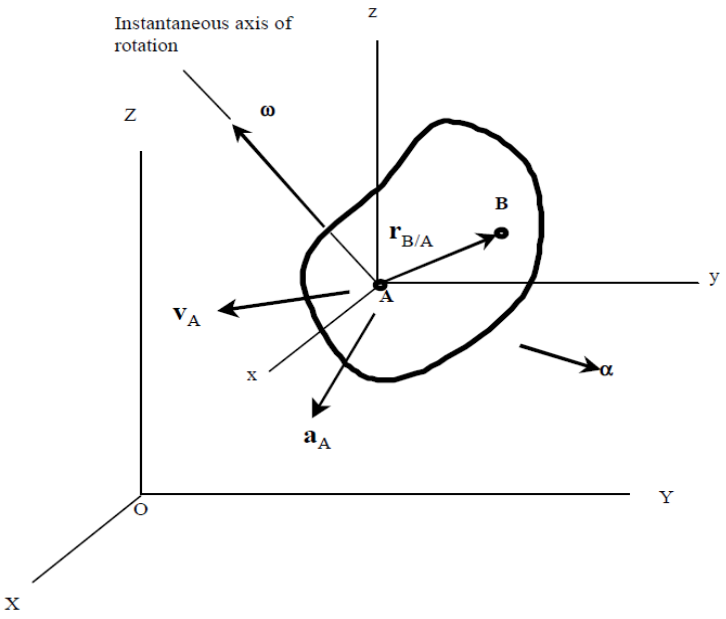

Figure 3. - Rigid Body assumption[23]

Motion happens around global center of rotation explained by:

$v_{B/A} = w \times r_{B/A}$ (1)

$a_{B/A} = a \times r_{B/A} + w \times (w \times r_{B/A})$ (2)

$v_{B/A}$ and $a_{B/A}$: The relative velocity and acceleration of point B with respect to point A.

r: Position relative to origin point

a: Acceleration

$v_B = v_A + v_{B/A}$ and $a_B = a_A + a_{B/A}$

$v_B = v_A + w \times r_{B/A}$ (3)

$a_B = a_A + a \times r_{B/A} + w \times (w \times r_{B/A})$ (4)

As a result, equation 4 can be written as [23]:

$$\begin{bmatrix} a_{Bx} \\ a_{By} \\ a_{Bz} \end{bmatrix} = \begin{bmatrix} a_{Ax} \\ a_{Ay} \\ a_{Az} \end{bmatrix} + \begin{bmatrix} \alpha_y r_z - \alpha_z r_y \\ \alpha_z r_x - \alpha_x r_z \\ \alpha_x r_y - \alpha_y r_x \end{bmatrix} + \begin{bmatrix} \omega_x(\omega_y r_y + \omega_z r_z) - r_x(\omega_y^2 + \omega_z^2) \\ \omega_y(\omega_z r_z + \omega_x r_x) - r_y(\omega_z^2 + \omega_x^2) \\ \omega_z(\omega_x r_x + \omega_y r_y) - r_z(\omega_x^2 + \omega_y^2) \end{bmatrix} \quad (5)$$

As seen in equation 5, algorithm provides to transform a_A to a_B. This analogy can be simply made for a_{mouth} to a_{cg}. In this project, results will give head landmarks positions relative to IMG such as r_x, r_y and r_z in equation 5. With these results, transformation algorithm can be used for to calculate a_{cg} as primary goal at the beginning of project[23].

CHAPTER II

MATERIALS & METHOD

MATERIALS

2.1. IMG HARDWARE

The Intelligent Mouthguard Printed Circuit Board (IMG PCB) contains:

- One 1Megabit Serial Peripheral Interface Memory Module,

  Model: 25AA1024,

  Manufacturer: EEPROM Microchip Technology Inc.

- One onboard microcontroller,

  Model: dsPIC33FJ128GP804,

  Manufacturer: Microchip Technology Inc.

- One three-axis MEMS angular rate sensor

  Model: L3G4200D

Manufacturer: ST Microelectronics

- Three single axis micro electromechanical systems (MEMS) linear accelerometers

  Model: ADXL001-250

  Manufacturer: Analog Devices

They all mounted to a flexible PCB which can be seen on **Figure 2**.

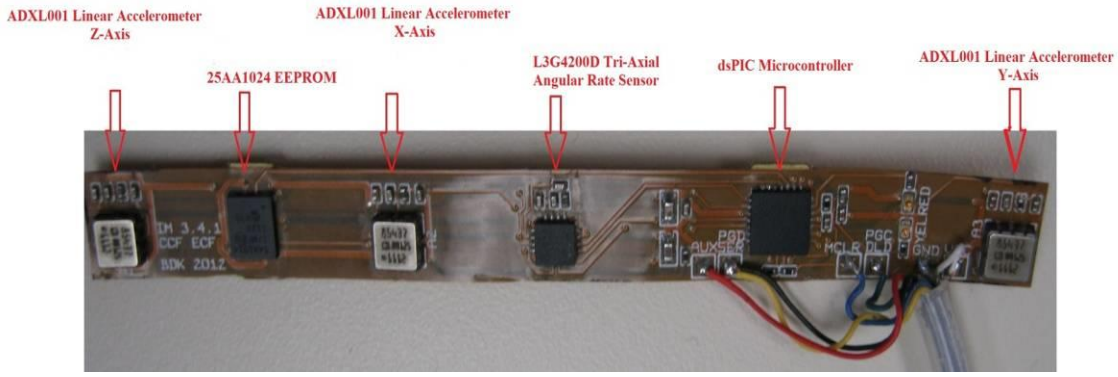

Figure 4. - dsPIC33 Microcontroller, ADXL001-250 Linear Accelerometers and ST Micro LG4200 Gyroscope Mounted on Circuit Board

2.1.1. ADXL001-250 Linear Accelerometers

Included are three (3) linear accelerometers (ADXL001-250, Analog Devices, Massachusetts USA) organized in a known pattern when laid flat, but arbitrary locations/orientations when inserted into the mouth. Each linear accelerometer produces an analog output voltage proportional to linear acceleration in the

sensing range of 0 to 250 g. Some properties of the accelerometer are shown below:

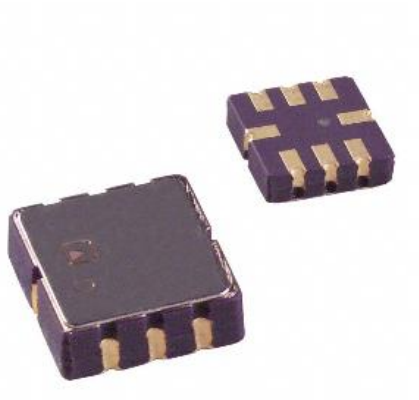

Figure 5. - Analog Devices ADXL001-250 Linear Accelerometer [9]

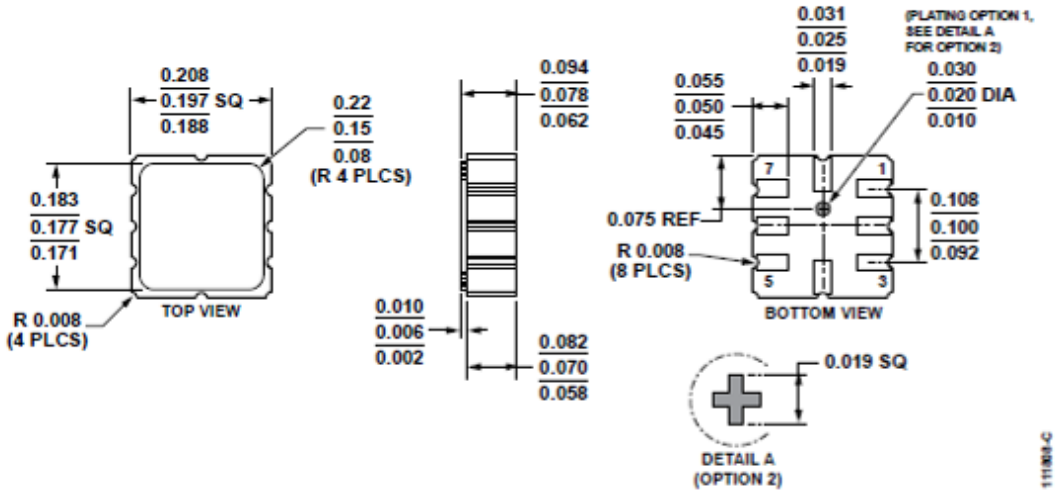

Figure 6. - Analog Devices ADXL001-250 Dimensions[9]

2.1.2. ST Micro LG4200 Gyroscope

3 axis (MEMS) gyroscopic sensor is used on IMG PCB.

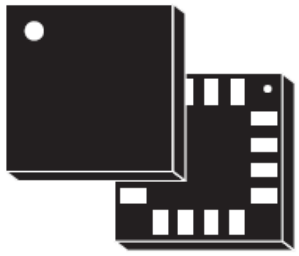

Figure 7. - ST Micro LG4200 Gyroscope Dimensions [10]

2.2. IMG POSITION

In this project, ADXL001-250 Linear Accelerometers and ST Micro LG4200 Gyroscope are sensors that must be located. Position and orientation of these sensors help to make very accurate measurement when impact occurs. To accurately quantify peak values of head impacts or concussions, orientation and position of each sensor relative to the CG (Center of Gravity) of human head must be calculated.

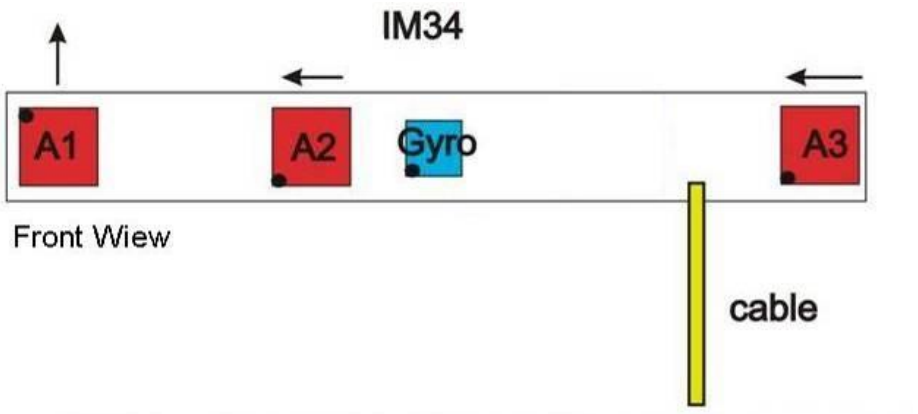

Figure 8. - ADXL001-250 Linear Accelerometers (A1-3)
and ST Micro LG4200 Gyroscope(Gyro) position on Circuit Board

PCBs should be mounted into plastic mouth guards molds so that every human subject can use it. Therefore, specific flexible printed circuit boards have been used in the project. Flexible PCBs are resistant to bending. They are durable against chewing, squeezing and stretching.

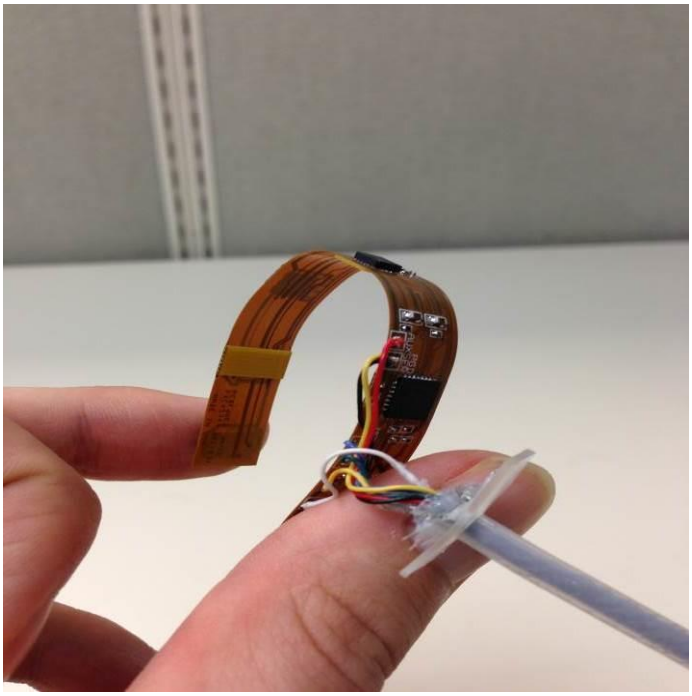

Figure 9. - Flexible Printed Circuit Board

2.3. IMG ORIENTATION

The orientation of IMG sensitive axes are defined based on SAEJ211 standards [6], as shown in **Figures 8, Table 1 and 2**.

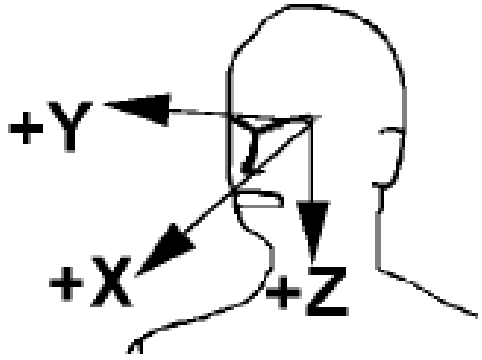

Figure 10. - Positive polarity directions

On-PCB	SAE J1734	Manipulation
GyroX	+MZ	Chin toward RIGHT shoulder
GyroY	+MY	Chin away from sternum
GyroZ	+MX	Right ear toward Right Shoulder

Table 1. - Angular velocity sensitive axis orientation

On-PCB (Linear Accelerometers)	SAE J1734	Manipulation
A1(-)	+Z	Translate Down (Cranial-Cadual)
A2(+)	+Y	Translate Left to Right
A3(+)	+X	Translate Forward

Table 2. - Linear accelerometer sensitive axis orientation

2.4. CAD Drawing and MRI PCB's

In order to determine position and orientation of IMG sensors, the IMG had to be scanned on MRI. Since IMG has electronic sensors and electrical connections, it was not able to be scanned because MRI properties require that no metal be present in the magnetic scanning field. Therefore, artificial IMG PCB which has same circuit design and same sensor locations was created from a technical drawing (See **Appendix D**) and 3D printed with MRI visible material (Fullcure 705). The 3D printed IMG PCB was named as "MRI PCB".

In production process of MRI PCB, the 3D model of IMG was created on Solidworks 2012. It is called "CAD Image". After the 3D model was created on software, a 3D printing machine (Objet Connex 350) was used to produce "MRI PCB".

Figure 11. - 3D Printing Machine, Objet Connex 350.

The Objet350 Connex 3D Printer has a support material called" FullCure 705" which is a non-toxic gel-like photopolymer support.

A number of designs and materials were tried with the 3D printing machine in order to obtain the best signal to noise ratio of the MRI PCB. The first design used oil filled sensors to approximate the signal contrast of fat, which has high contrast using T1 weighted MRI.

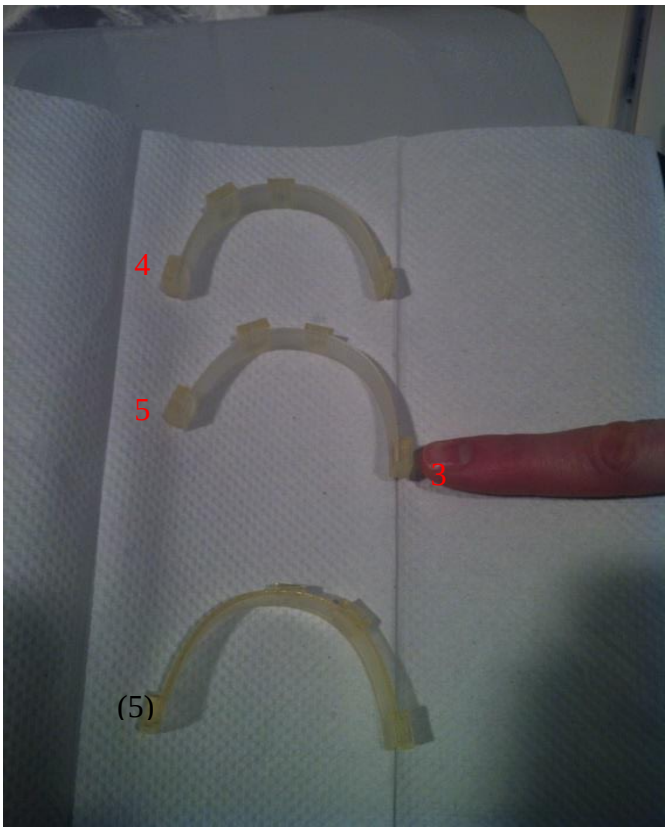

Figure 12. - Sensors volume filled with Oil (MRI PCB v1.0)

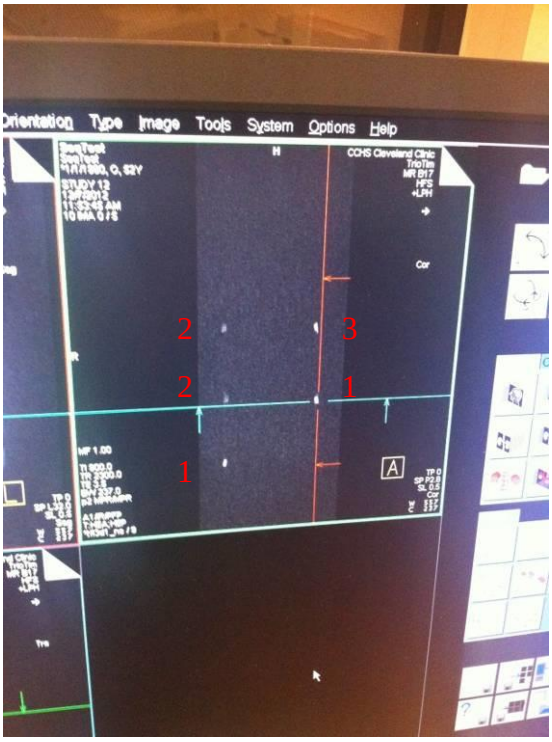

Figure 13. - Appearance of sensors volume on MRI Scan with same numbering

In the oil-filled design, only 4 sensor positions are visible and it was difficult to segment sensors from background. Another approach was creating a volume for MRI PCB and filling it with oil instead of filling only the sensor volume. With this design the MRI PCB volume appeared on MRI and sensors volume remained as voids.

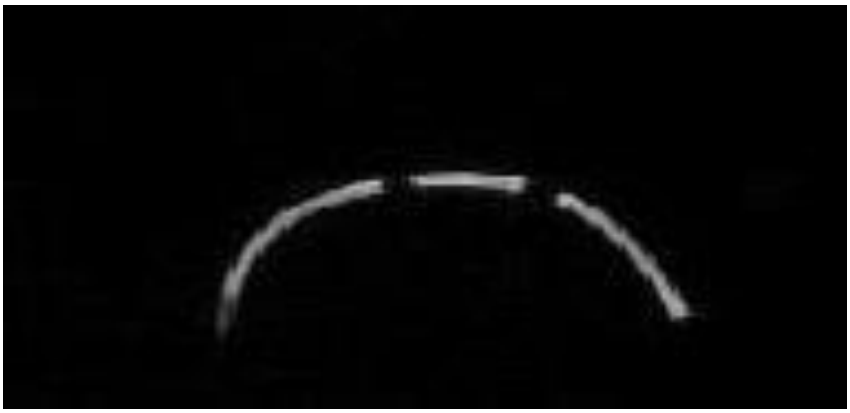

Figure 14. - Appearance of MRI PCB volume with oil, sensors void on MRI Scan (MRI PCB v2.0)

To determine sensors' position and orientation, it was observed that filling the volume with oil was not the perfect method. Despite the fact oil considered as a good MRI visible material, it did not give enough accurate results. Because of the properties of oil and permeability of the outer MRI PCB material, it leaked or the surrounding layer of MRI PCB absorbed oil. This caused some non-visible areas on the MRI PCB volume and distorted the PCB edges. Therefore, a new material, Fullcure705 was used in order to produce the final MRI PCB v3.0. Fullcure705 is actually a supporting material of 3D Printing Machine, Objet Connex 350, and is typically washed away with water after 3D printing is completed. But during one MRI it was discovered that Fullcure 705 was a very good MRI visible material, on par with oil. Also it was solid when it cured and did not pose risk of leaking or osmotic diffusion like oil.

2.4.1. Features of Fullcure 705

Fullcure 705 is made of acrylic based photopolymer material. It usually provides precise and detailed 3D models. It can be used in rapid prototyping applications. This material is like a gel and this feature provides elasticity which is important to create shape of MRI PCB. Since Fullcure 705 has water like features, this feature offer free protons for the MRI to use in imaging. Its feature provides bright whiteness on T1 weighted images as it is required in this project. (See **Appendix A** for Datasheet of Fullcure 705).

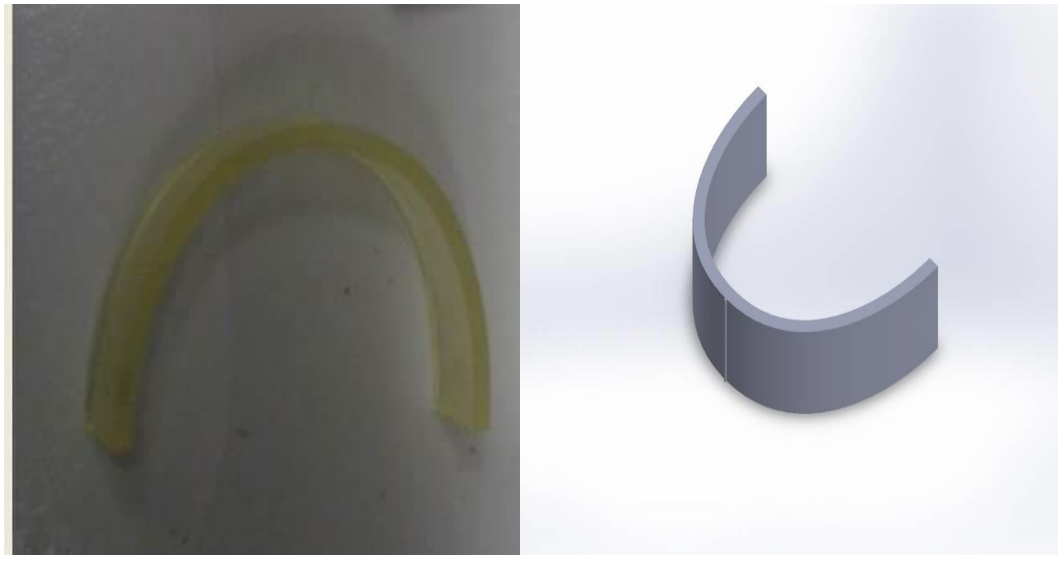

A) B)

Figure 15. - A) Rigid MRI PCB (version 3.0)
B) CAD Drawing of Rigid MRI PCB

A Rigid, curved, MRI PCB was designed for Validation Part It was built to nearly the same dimensions as the CAD drawing shown in **Figure 13B**. However,

the ultimate goal of this project was to identify sensor's position and orientation of MRI PCB during human use. Therefore, a "Human MRI PCB" was built from the same dimensions by using flexible "Fullcure 705" material. "Human MRI PCB" was sealed and made like a mouthguard so that a human volunteer was able to put it in his mouth as shown in **Figure 14**.

Figure 16. - Human MRI PCB; a flexible version of the rigid MRI PCB version 3.0 is sealed within a custom EVA mouthguard

2.5. MRI OVERVIEW

Magnetic Resonance Imaging (MRI) comes from the hydrogen atom because of its magnetic. If it interacts with a large magnetic field and radio waves, interaction creates detailed images of the human body. To use MRI, it is need to have a strong magnetic field.

Each substance of the body has different tissue relaxation time. Because, there are different chemical patterns and different radiation levels for each tissue. This radiation levels difference is detected by MRI machine and it will be transformed into electrical current. Then electrical current is used to construct the image. There are three types of magnets which are used for MRI. These are called permanent, resistive and superconductive magnet. Permanent magnet has been used in this project.

"Brain Mapping" research area is one of top topics recently. "Functional Magnetic Resonance Imaging" is the newest tool which has been used in this area and it provides the best volumetric picture of the human brain.

Figure 17. - Siemens Magnetom Trio 3T MRI Machine

METHOD

2.6. MRI PROTOCOL

As MRI scanning protocol of MRI PCB, MRI protocol of Alzheimer's Disease Neuroimaging Initiative (ADNI) study was used. ADNI is a worldwide research foundation which works for to investigate the progression of Alzheimer's Disease. ADNI researchers use established, standardized MRI protocol in order to investigate the progression of Alzheimer's Disease. In this project, Siemens Magnetom 3T was used as MRI machine.[20].

2.7. VALIDATION PART 1 (MRI Images vs. CAD Drawing)

In Validation Part 1, the Rigid MRI PCB was scanned on the MRI and compared with the CAD Image. This part validated the proper procedure to extract position and orientation information of MRI PCB sensors using MRI images.

Validation Part 1 consisted of comparing the CAD Image and MRI PCB data via custom written MATLAB code. As a result of Validation Part 1, sensors position and orientation of MRI PCB was documented with respect to CAD Image position and orientation data.

2.7.1. CAD Image

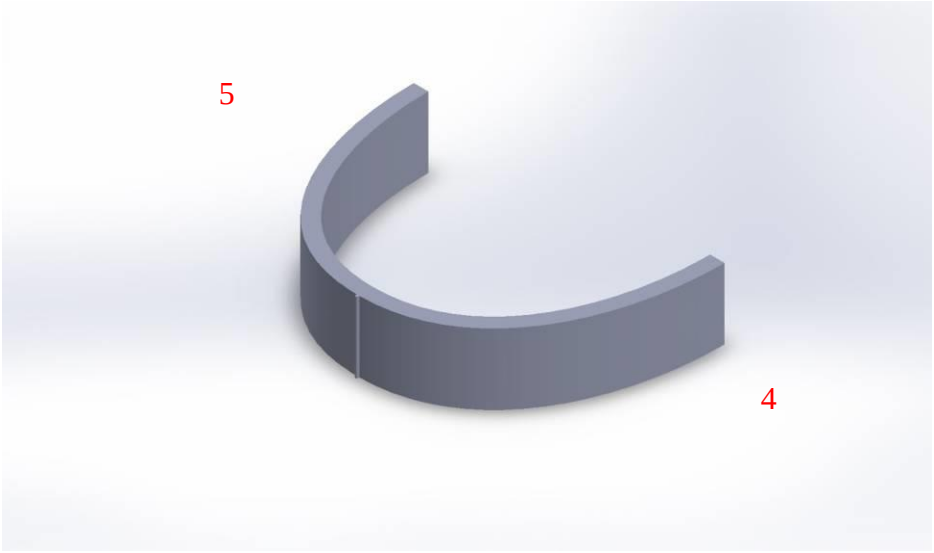

Figure 18. - CAD Image of Rigid MRI PCB

As a first step, the CAD Image (.TIFF) file was imported to MATLAB software as reference and pixel points of drawing were extracted.

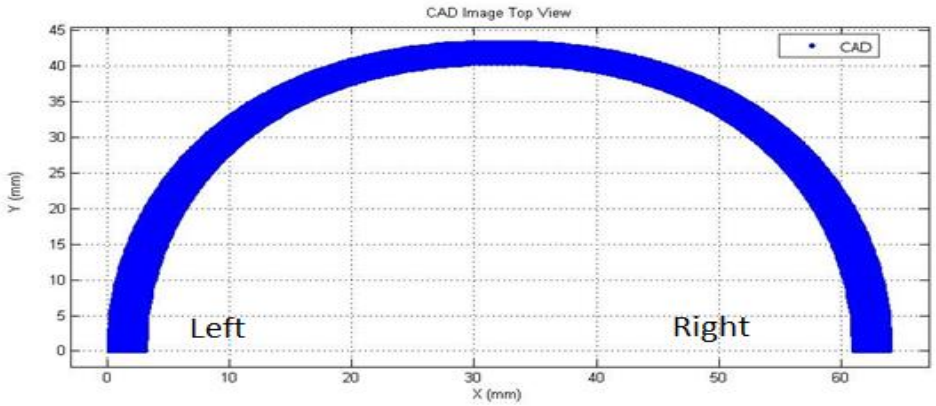

Figure 19. - CAD Image of Rigid MRI PCB imported to MATLAB

The CAD Image and Rigid MRI PCB were compared in two views. One view was a top view to compare the shape of two images and the other view was a transverse view cutting through PCB half of it so that all sensors can be seen.

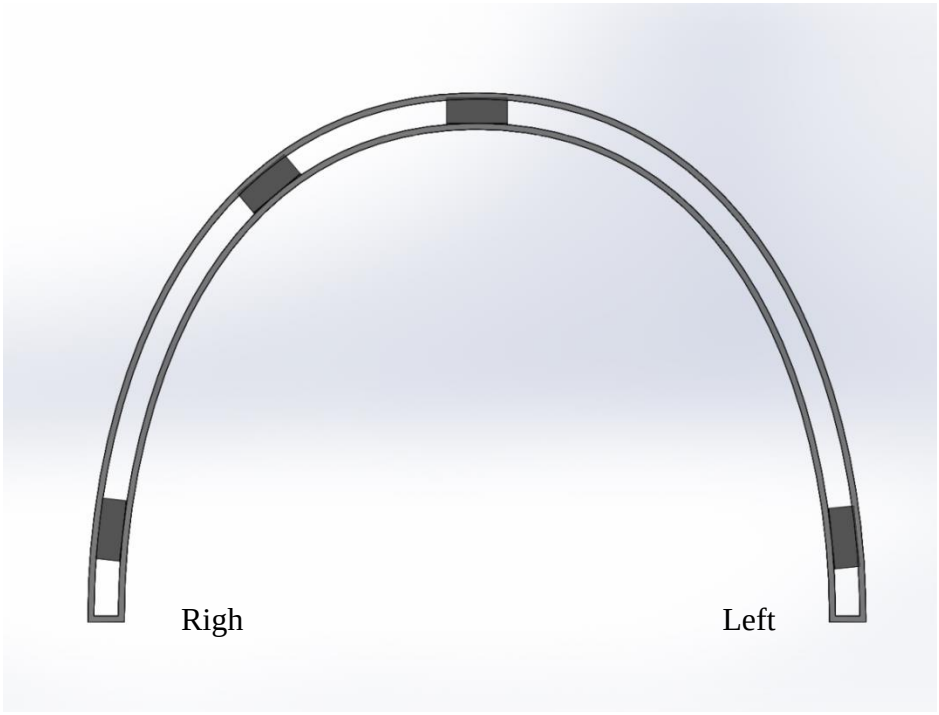

Figure 20. - Transverse Cross section View CAD Image of Rigid MRI PCB

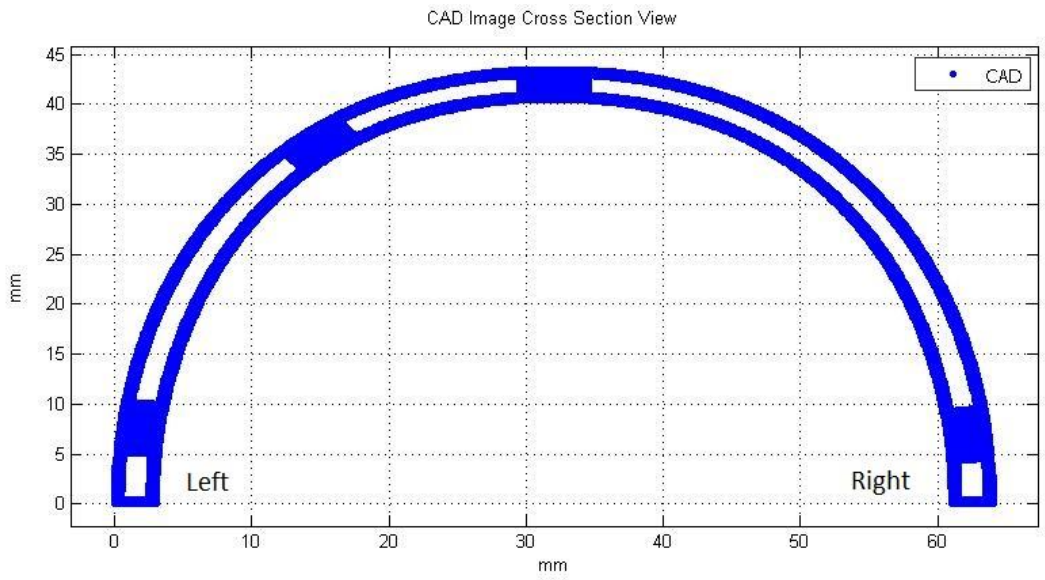

Figure 21. - CAD Image Cross Section View imported to MATLAB

At the end of this part, the top view and cross section view of CAD Image were obtained by importing the drawings into MATLAB software.

2.7.2. MRI Image of Rigid MRI PCB

In this part, the purpose was to obtain the same type of data as in the **Section 2.7.1.**

Since the ultimate goal of Validation Part 1 was to compare CAD Image with "Rigid MRI PCB", the "Rigid MRI PCB" was scanned and MRI Images were processed on MATLAB with custom written code.

Figure 22. - Rigid MRI PCB

Figure 23. - Rigid MRI PCB while scanning

Some processes had to be applied in order to extract only MRI PCB from MRI Image. Before determining sensors' position and orientation, clearing, cropping and intensity change processes were done.

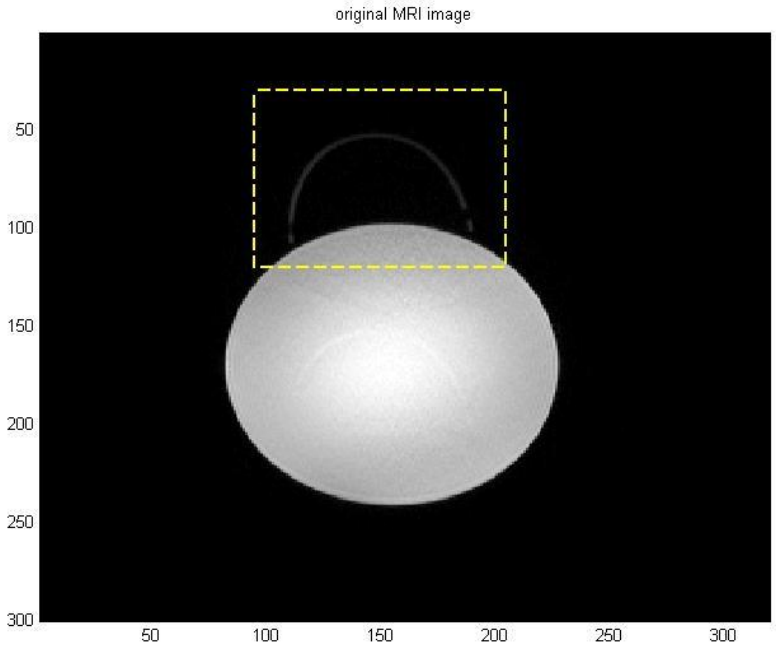

Figure 24. - Raw MRI Image, Slice No : 58

As shown in **Figure 24,** the raw MRI image had some noise and unrelated areas from Rigid MRI PCB. A clearing process was done by simply determining threshold value for pixels. The threshold value was determined according to Rigid MRI PCB's pixel values. After removing noise, the image was cropped to the region of interest.

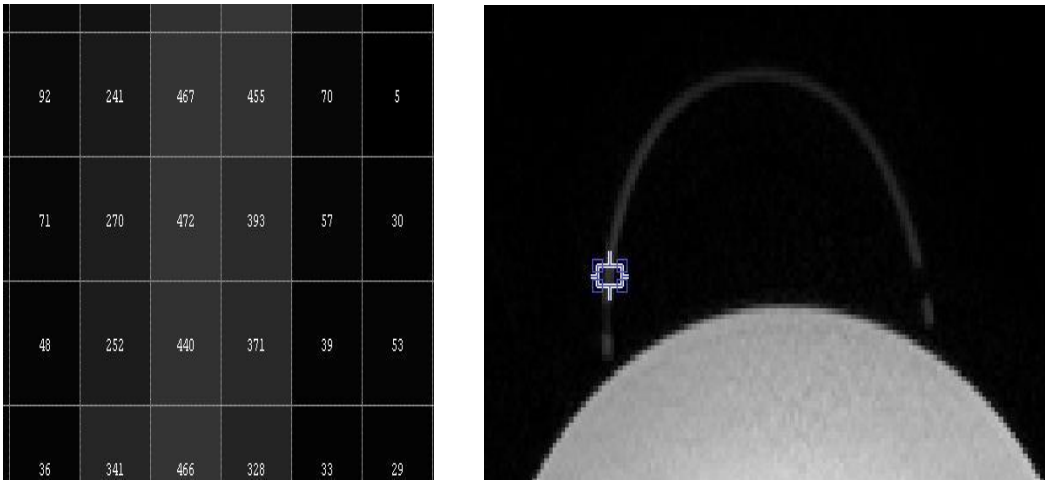

A B

Figure 25. - Identifying proper pixel value for threshold.

A) Pixel value of marker on B

B) Cropped Image of Raw MRI Slice No: 58

After removing noise and cropping, the same procedure was applied all three axis views (transverse, coronal and sagittal plane). Since there were multiple numbers of slices in all three planes, a reconstruction process was applied in order to build the 3D model. **Figure 26** shows one of the slices in coronal plane while the image reconstruction process was applying.

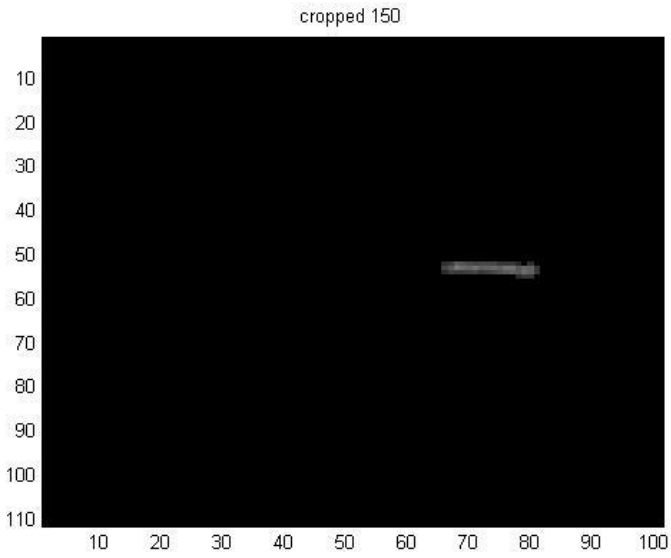

Figure 26. - Slice No:150 in coronal plane during image reconstruction process

After image reconstruction was done, it was noticed that “Rigid MRI PCB” was not perfectly aligned with the X-Y-Z axes that coincided with the MRI machine global coordinate system. Therefore, it was decided to reorient “Rigid MRI PCB” and perfectly align the PCB axes with J211 axes. An Euler Angle transformation process was implemented in this step.

2.7.2.1. Euler Angle

In order to determine the orientation of a rigid body, the Euler angles established by Leonhard Euler are used [12]. There are three parameters need to be specified in order to describe orientation in 3-dimensional space. Representation signs are α, β, γ. With these three signs, user can define any type of orientation of vector. For instance:

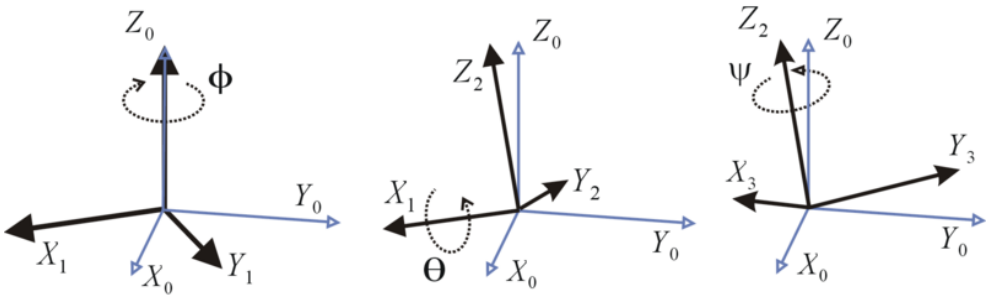

Figure 27. - 3 angle needs to be known to complete an Euler Transformation [13]

In this project, system coordinate frame is a right-handed Cartesian frame. The unit vectors are x,y,z which can be visualized in MATLAB using the below script:

```
function dcm = Euler(roll, pitch, yaw)
    cR = cos(roll);  sR = sin(roll);
    cP = cos(pitch); sP = sin(pitch);
    cY = cos(yaw);   sY = sin(yaw);

    dcm = [cP*cY           cP*sY           -sP;
           sR*sP*cY-cR*sY sR*sP*sY+cR*cY sR*cP;
           cR*sP*cY+sR*sY cR*sP*sY-sR*cY cR*cP];
end
```

Figure 28. - Custom written MATLAB code for Euler Matrix

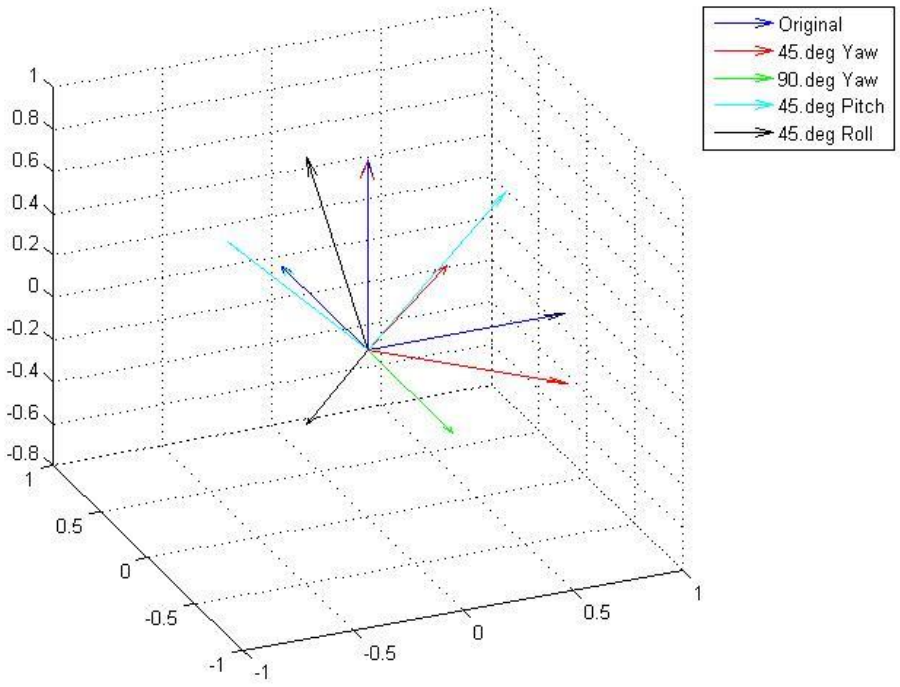

Figure 29. - Coordinate system transformation according code from **Figure 29**

As shown in the Figure 31, custom written script about Euler Transformation Matrix was used to reorient **Figure 30**.

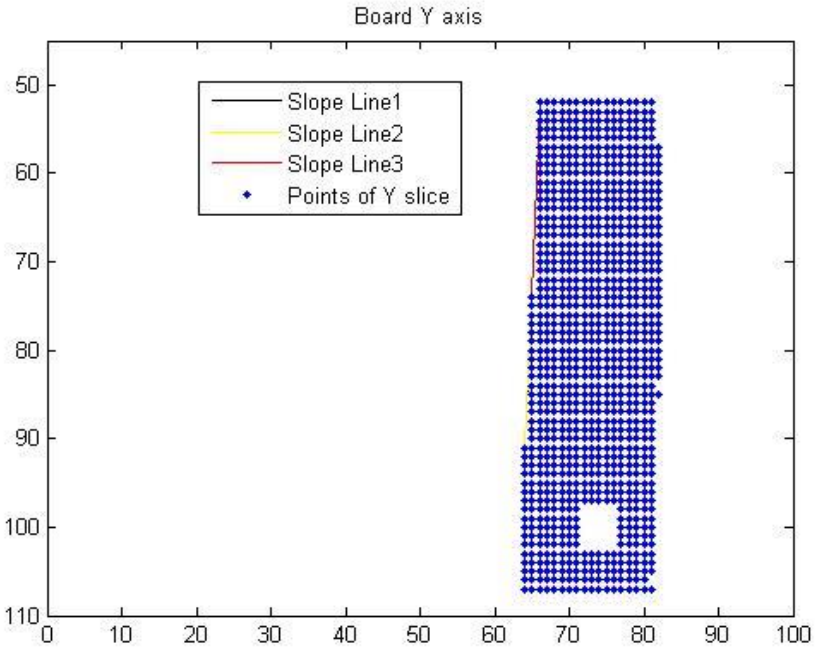

Figure 30. - Image reconstruction of “Rigid MRI PCB”

As seen in Figure 31, one side of the Rigid MRI PCB was reconstructed from coronal plane slices.

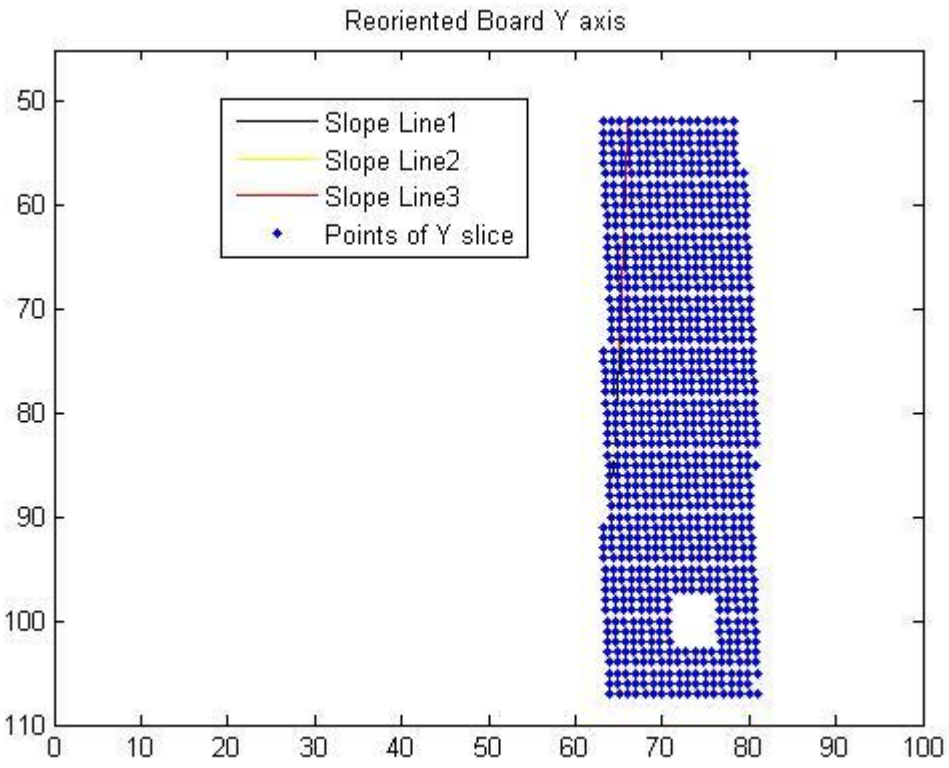

Figure 31. - Reoriented Coronal view of “Rigid MRI PCB”

At the end of Validation Part1, the mentioned procedure was applied to all three plane and all slices. A 3-D Model of “Rigid MRI PCB” was reconstructed with this procedure. The results are shown in **Section 3.1.**

2.8. VALIDATION PART 2 (Human MRI Image)

The purpose of Validation Part 2 was to validate that the procedure described in Validation Part 1 is applicable for Human MRI. In Validation Part 2, sensor position and orientation of the Flexible MRI PCB were determined and distance to CG of head from sensors position was calculated.

Human MRI PCB was sealed and made as a real mouthguard using clear ethyl vinyl acetate (EVA) “Polyshok” material. The Human MRI PCB was positioned within the mouthguard with the gyroscope at the center, and the PCB in approximately the same position as the IMG used in on-field data collection. This mouthguard was then given to volunteer for MRI scanning. The volunteer was scanned according to protocol described in **Section 2.7.6.2**

Figure 32. - Human MRI PCB

Figure 33. - Volunteer putting Human MRI PCB in his mouth before MRI scan

After MRI scanning procedure was done the data were processed using custom written code implemented in MATLAB software. A custom GUI and the same written code from Validation Part 1 were used for processing the Volunteer's MRI Images.

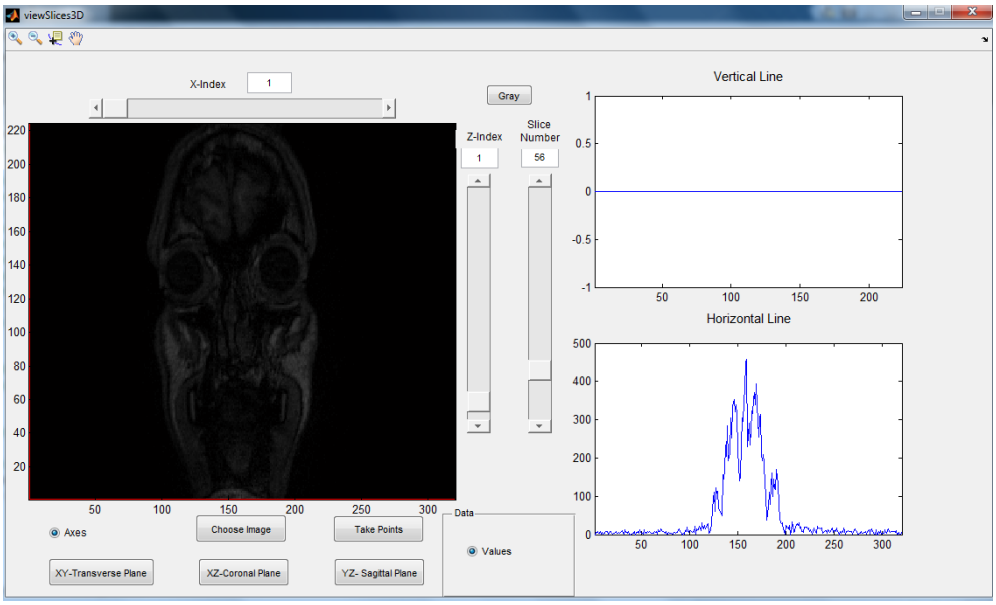

Figure 34. - Custom GUI specifically designed for Human MRI Scan

In this GUI, the Transverse, Coronal and Sagittal Planes can be seen slice by slice. Also, two index tools are provided to measure pixel values on the horizontal and vertical axes.

Since the Human MRI PCB had lower contrast between itself and surrounding tissues, the area around Human MRI PCB was manually cleared on all transverse, coronal and sagittal plane. This process can be seen in **Figure 35** as an example**.** After this process, the same procedure in Validation Part 1 was applied in order extract the Human MRI PCB from MRI slices. A total of (50) slices were used during this extraction process.

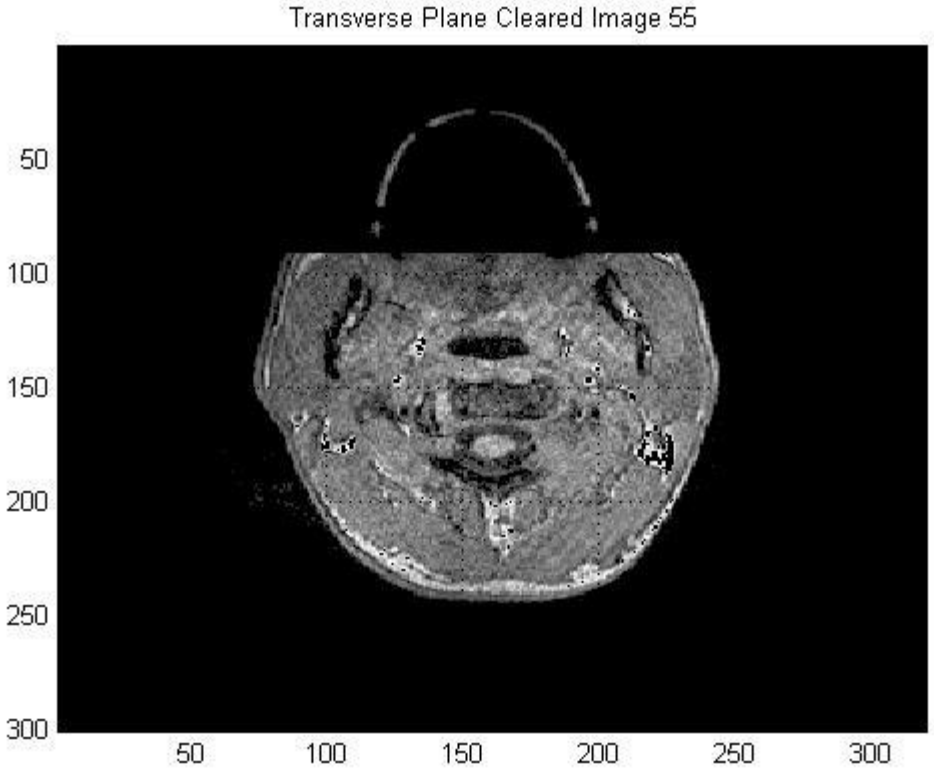

Figure 35. - View of Slice No: 140 in sagittal plane while extracting Human MRI PCB

After the Human MRI PCB was extracted, as a next process the CG of head was calculated. To calculate the CG of head, some anatomical landmarks had to be defined.

2.8.1. Determining the Frankfurt Plane:

The first step to determine the center of gravity of human head is finding the Frankfurt Plane. The determination of Frankfurt Plane has been made as the anatomical position of the human skull.

As shown in **Figure 36**, the Frankfurt plane is an anatomical plane which is parallel to the transverse plane trough the orbitale-tragion line. The Frankfurt plane is defined by three points comprising the left orbitale (lower margin of the left eye socket) and external auditory meati (left and right). The tragion, which lies just cranial and anterior to the external auditory meatus, is used as the Frankfurt plane origin when projected onto the mid-sagittal plane [7].

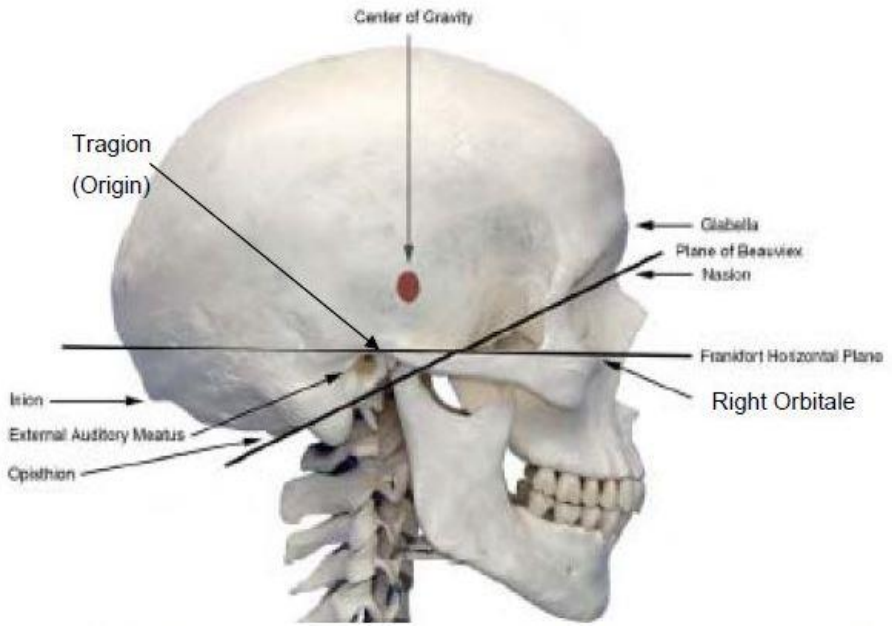

Figure 36. - Frankfurt Plane: Comprised of a plane parallel to the transverse plane through the left and right auditory meati, and left orbitale [14]

The human head CG has been commonly referenced to the Frankfurt Plane and tragion; hence, the head CG lies in the mid-sagittal (XZ) plane in an area 2.6±0.7cm superior (in –Z direction) and 0.7±0.6cm anterior (in +X direction) to the origin in the mid-sagittal plane (See **Appendix C**)

To extract the Frankfurt plane, a custom written GUI was used. Since the GUI was user friendly, 3 points (left orbitale, left and right auditory meati) required to determine the Frankfurt plane could be selected in any slice. When the user selected a point,the “Take Points” button on the custom GUI was used.

The process for selecting the three Frankfurt Plane points from the GUI is described further:

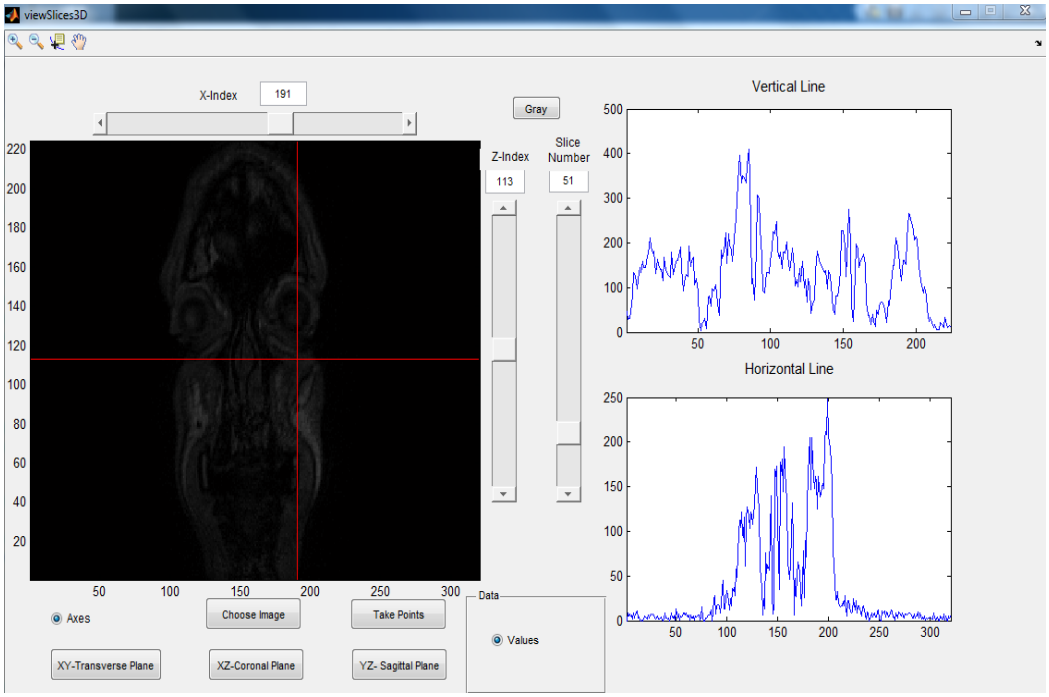

Figure 37. - Coronal Plane Slice No: 51, left orbitale was selected as the first point

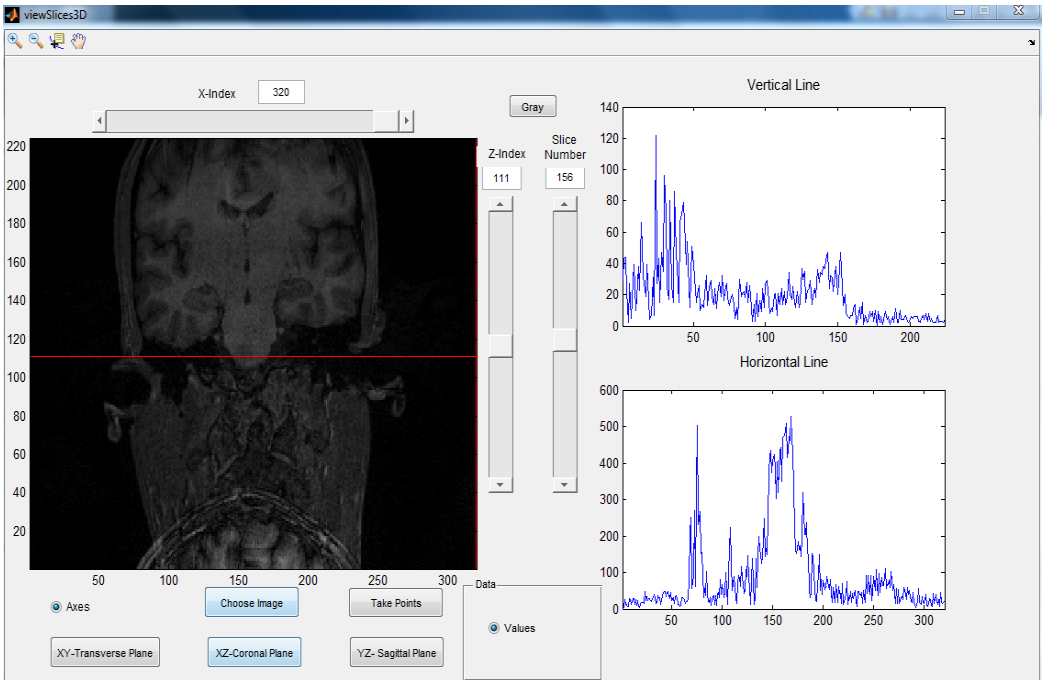

Figure 38. - Coronal Plane Slice No: 156, left auditory meatus was selected as the second point

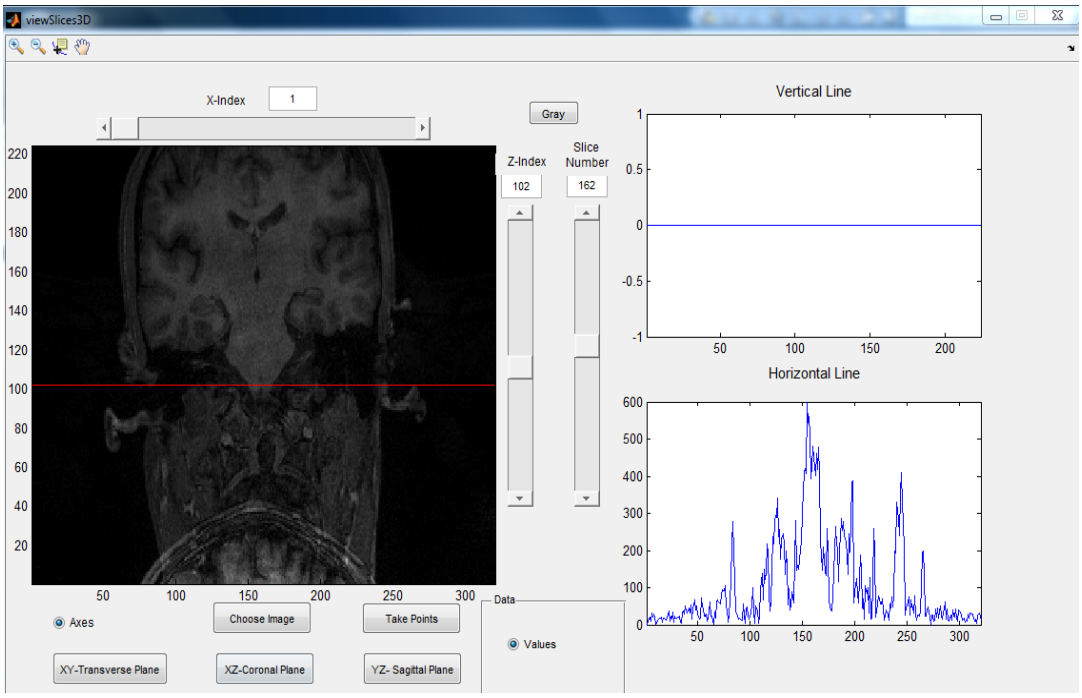

Figure 39. - Coronal Plane Slice No: 162, right auditory meatus was selected as the third point

After the 3 points were selected, a custom written MATLAB code extracted the Frankfurt plane and computed the CG location with respect to the MRI Image volume. At the end of Validation Part 2, sensor position and orientation of the Human MRI PCB with respect to the CG of head was determined and is shown in the results section.

CHAPTER III

RESULTS

3.1. VALIDATION PART 1 (Rigid MRI PCB vs. CAD Image)

In Validation Part1, the Rigid MRI PCB and CAD Image were compared with a custom written MATLAB code. The CAD Image was used as reference. As a first step, the CAD Image was processed as a reference. The top view and cross section view of the CAD Image are compared with the Rigid MRI PCB Slice No: 22 and Slice No: 11 below.

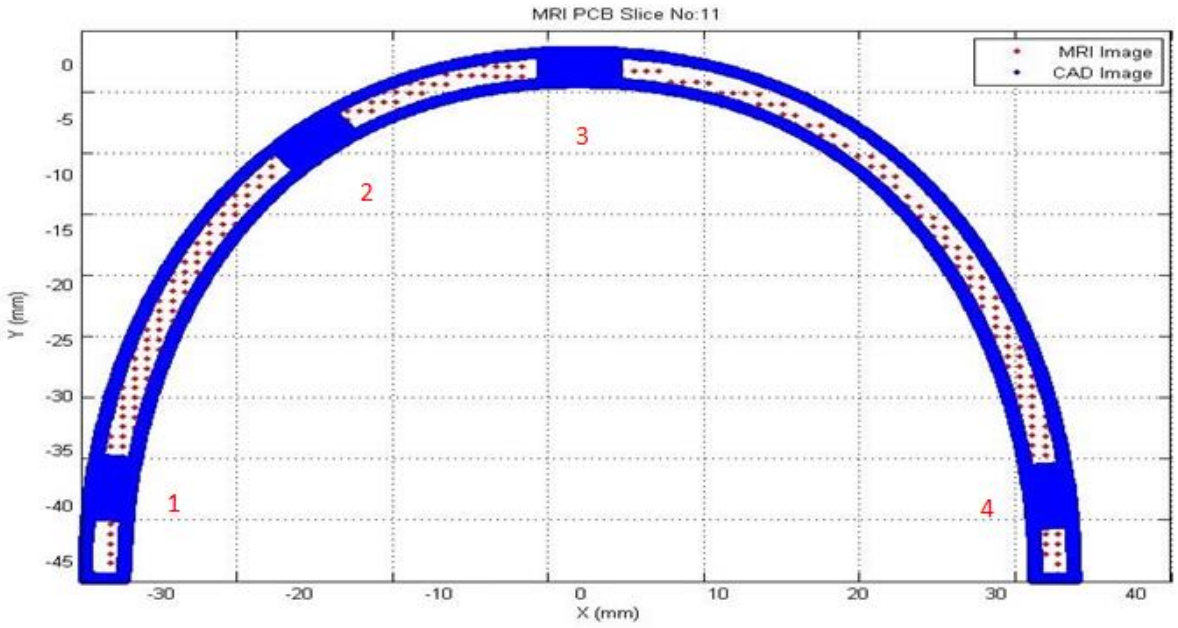

Figure 40. - MRI PCB Slice No:11 and Cross Section View of CAD Image.

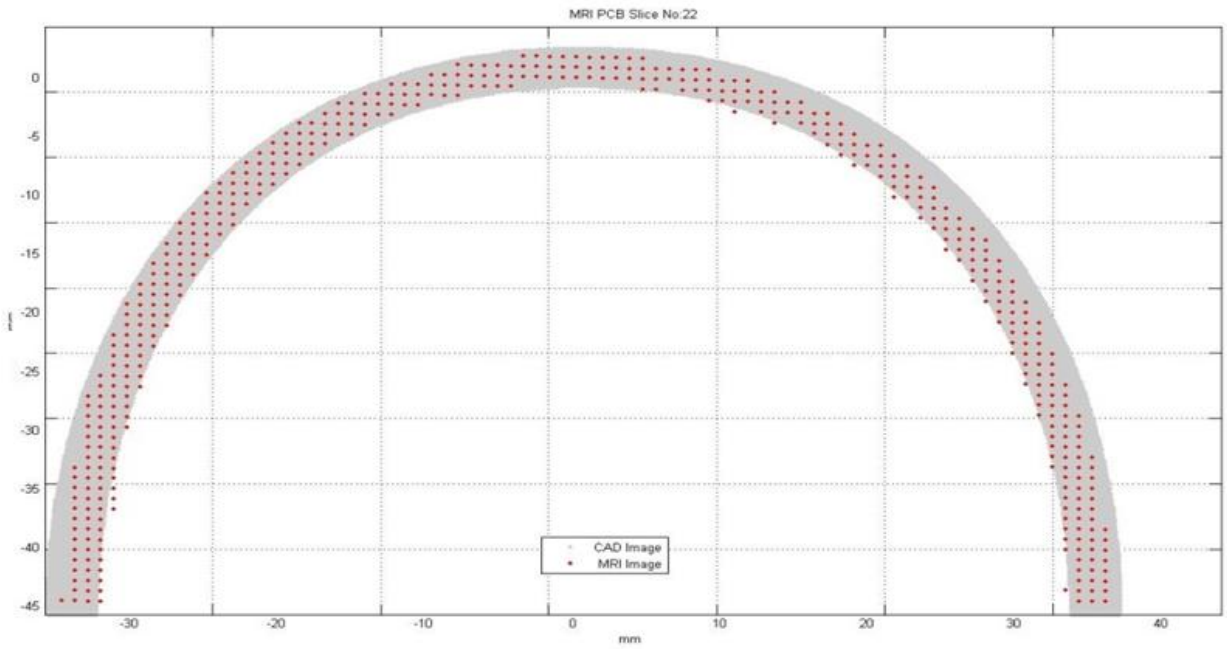

Figure 41. - MRI PCB Slice No:22 and Top View of CAD Image. This image shows the overlap between points extracted from the MRI PCB in comparison with known dimensions for the CAD Image of the IMG PCB.

The X (medial-lateral) positions of the four sensors in the CAD Image were selected as constant reference values. The differences in Y values (anterior-posterior) and orientation changes were observed in MRI PCB Slice No:11 while X-values were increasing. All position values were measured in mm. The MRI PCB Slice No:11 was used to measure Y-values at each CAD X-value as this slice was the transverse bisector of the MRI PCB.

	CAD X (mm)	CAD Y (mm)	Y (mm) of MRI Slice No:11	Difference (mm)
Sensor1	-30.2	-34.2	-34.3	0.12
Sensor2	-17.3	-6.06	-6.51	0.45
Sensor3	0.00	0.10	-0.36	0.46
Sensor4	30.1	-34.7	-34.9	0.19

Table 3. - Y Position Values of MRI Slice No: 11 at X value of CAD Image

As mentioned in the "Method of Validation Part 1", Rigid MRI PCB was reoriented according to Euler calculations.

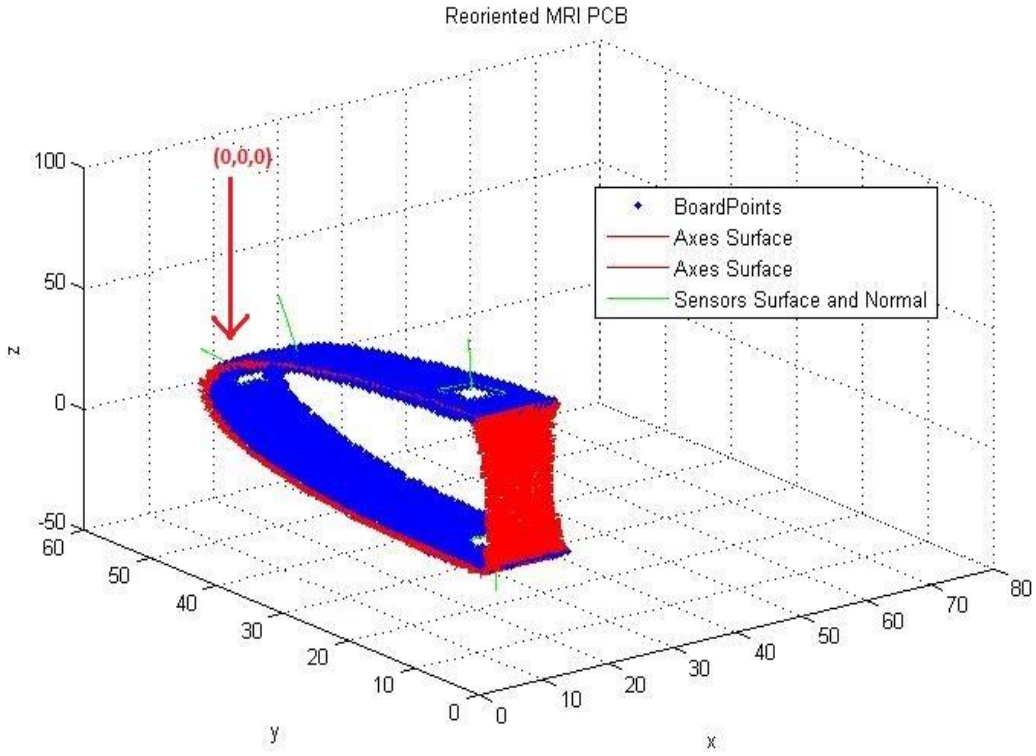

Figure 42. - Reoriented Rigid MRI PCB with positions and orientations for each sensor (noted by normal vector attached to each sensor surface)

The sensor positions with respect to the origin (shown in Figure 41 with the red arrow) are:

	Position(mm)		
	X	Y	Z
Sensor 4	0.99	-35.9	-28.6
Sensor 3	0.00	0.00	0.00
Sensor 2	0.01	-6.63	17.4
Sensor 1	-0.93	-34.2	34.2

Table 4. - Rigid MRI PCB positions with respect to origin

As mentioned in **Section 2.7.2.1**, three values for X-Y-Z were able to calculate orientation of normal vector of sensors. The Euler angle transformation matrix values are written below. They can be considered as inverse cosine values.

	Orientation (Euler Angles)		
	PHI (Yaw) X	THETA (Pitch) Y	PSI (Roll) Z
Sensor 1	0.1	-1.0	0.0
Sensor 2	0.7	-0.6	0.0
Sensor 3	1.0	0.0	0.0
Sensor 4	0.1	1.0	0.0

Table 5. - Rigid MRI PCB positions with respect to the origin

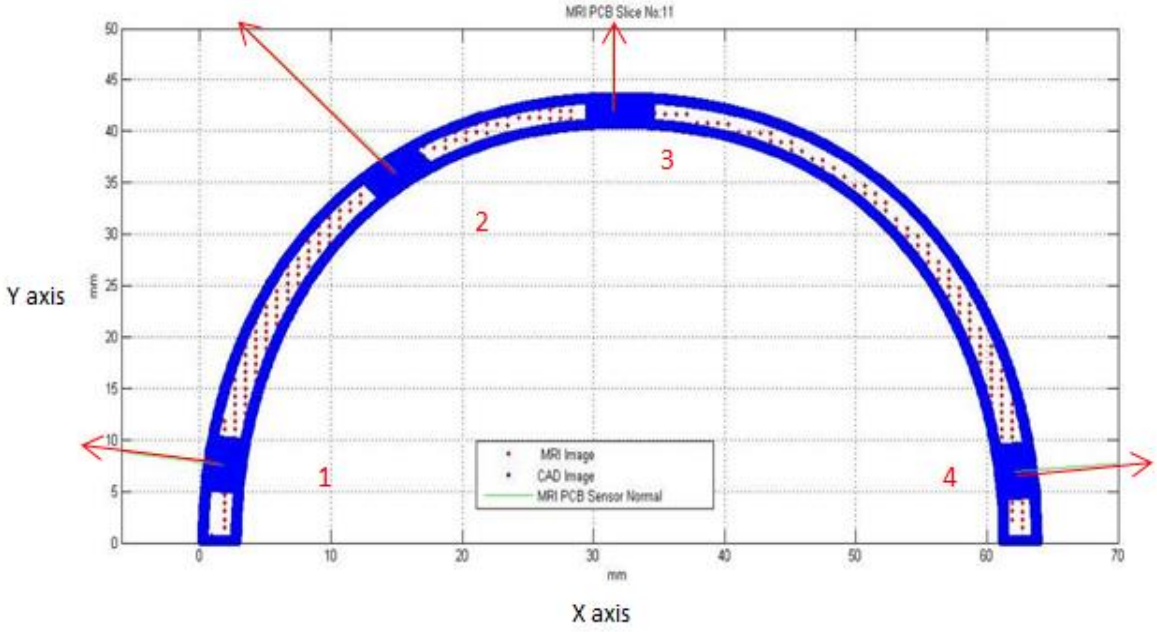

Figure 43. - MRI PCB sensors (solid blue areas) with normal vectors (shown by arrows), Slice No:11

If these Euler Transformation values were to convert to an angle, all sensors would have the same perfect normal vector angle (90°) as in the CAD Image. Hence, the orientation of the Rigid MRI PCB is shown as a change compared with the ideal CAD Image value of 90°.

	Normal Vector Angle on X axis (in degree°)			
	Sensor1	Sensor2	Sensor3	Sensor4
CAD Image	-7.32	-51.5	90.0	7.32
Rigid MRI PCB	-5.71	-49.4	90.7	5.74
Difference of Angle	1.61	2.10	0.68	1.58

Table 6. - Angle of normal vectors in CAD Image and change in normal vectors of MRI Slice No: 11

3.2. VALIDATION PART 2 (Human MRI Image)

The Frankfurt Plane was extracted after the reorientation process explained in **Section 2.7.8** (Validation Part 2)

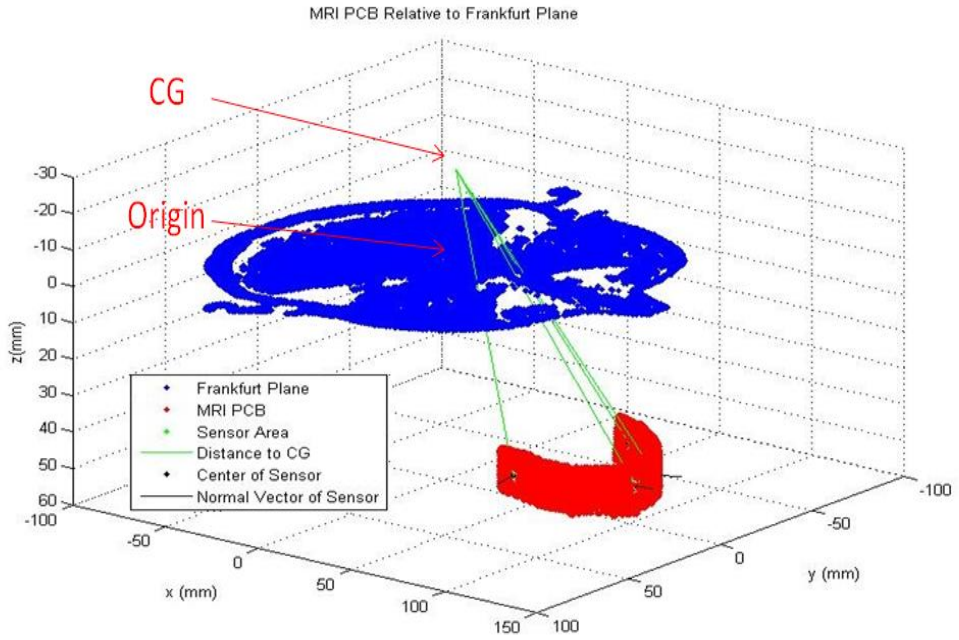

Figure 44. - Human MRI Scan with Human MRI PCB sensor positions and orientations

Sensor positions, orientations and distances to the CG of head are:

	Position from CG (mm)			Position from Origin (mm)			Orientation (Euler Angle)			Distance to CG
	X	Y	Z	X	Y	Z	PHI (Yaw) X	THETA (Pitch) Y	PSI (Roll) Z	(mm)
Sensor 1	61.3	32.2	73.6	68.3	32.2	47.6	0.17	-0.99	0.02	101
Sensor 2	90.2	18.0	76.5	97.2	18.0	50.5	0.84	-0.64	0.10	120
Sensor 3	97.1	-0.30	75.1	104	-0.30	49.1	1.00	0.00	0.10	123
Sensor 4	61.6	-30.4	70.8	68.6	-30.4	44.8	0.15	0.99	0.01	99

Table 7. - Human MRI PCB positions with respect to the CG of head.

The angle of the "Human MRI PCB" in three planes (transverse, coronal and sagittal) was calculated by creating a plane going through middle of all sensor locations.

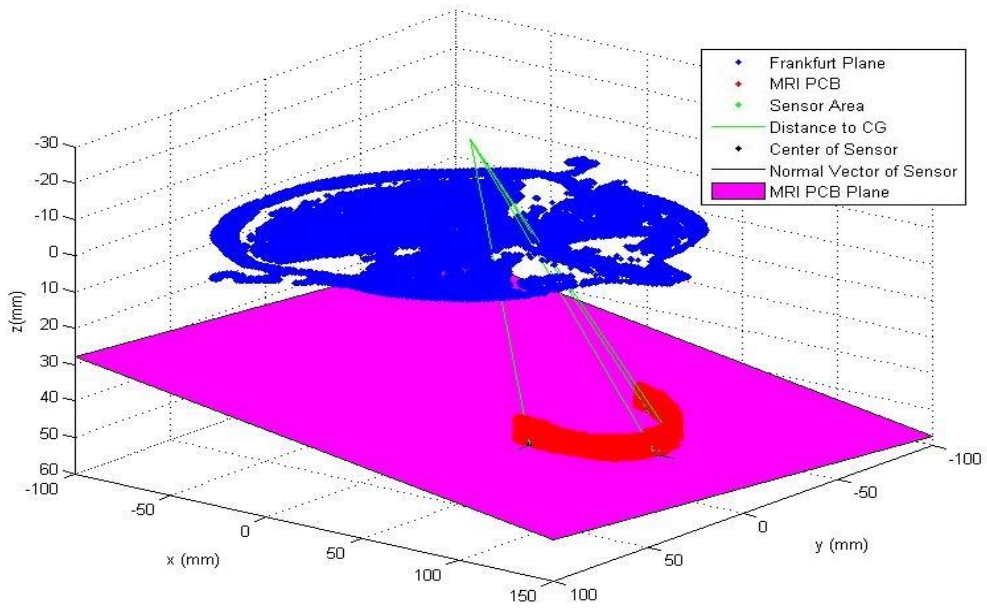

Figure 45. - Plane going through the middle of Human MRI PCB. Vectors from each sensor to the head CG are shown.

The angle of the “Human MRI PCB” in three planes (transverse, coronal and sagittal) was calculated from following three figures, each figure taken in a 2-D plane.

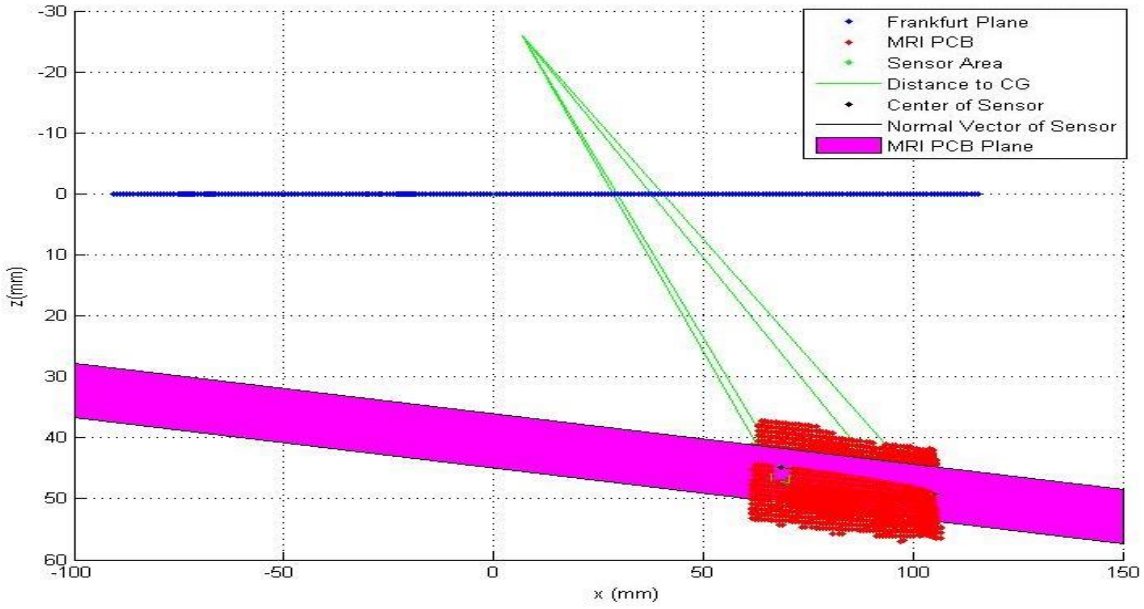

Figure 46. - The Frankfurt maxillary angle of the “Human MRI PCB” on the Sagittal (X-Z plane)was 6.8°.

The modified Hybrid III that is used in NFL mouthguard testing has a Frankfurt maxillary Angle of 10° [22]. However, according to **Figure 45**, Frankfurt MAXILLARY Angle was calculated as 6.8°.

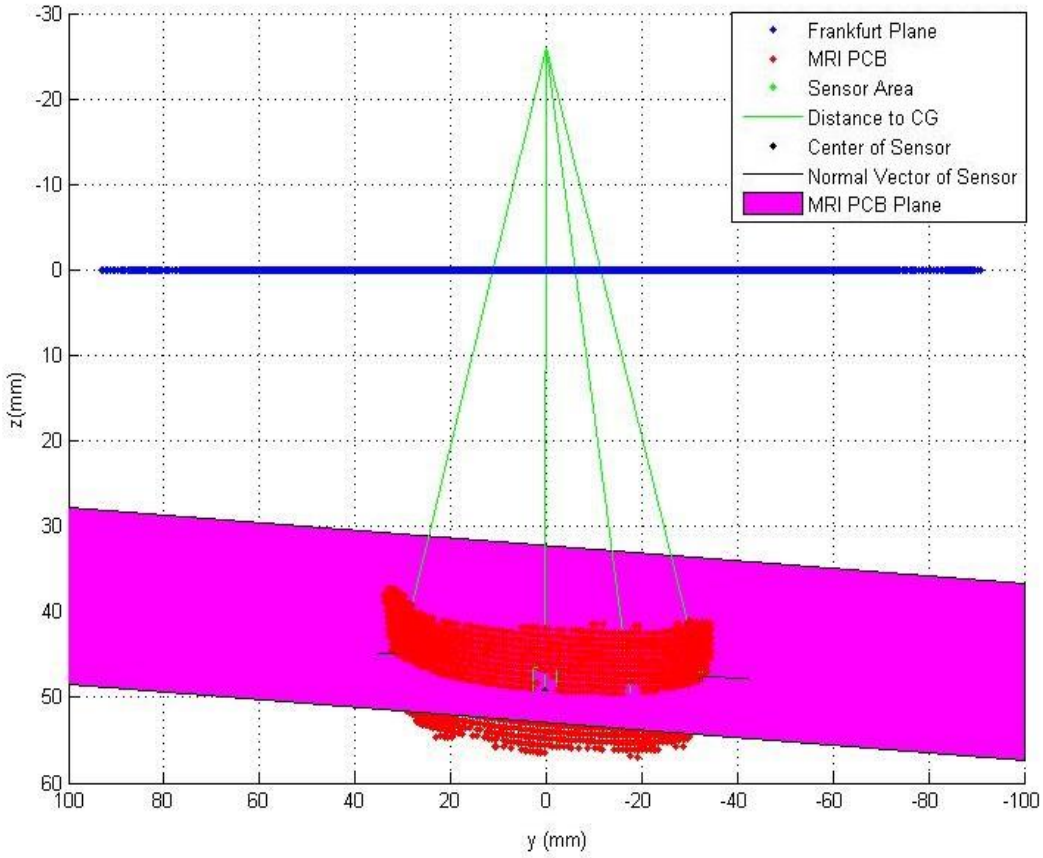

Figure 47. - The angle of the "Human MRI PCB" in the Coronal (Y-Z) plane was 2.6°.

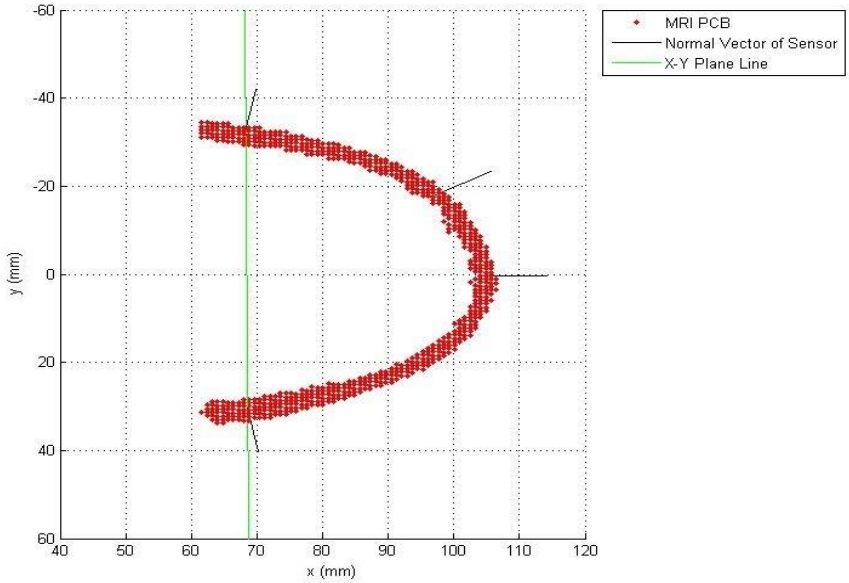

Figure 48. - The angle of the "Human MRI PCB " on the Transverse (X-Y) plane was 0.5°.

In the Transverse plane the CAD Image was re-oriented by 0.5° to allow direct comparison to the Human MRI PCB in **Figure 47.**

	Normal Vector Angle on Y axis (in degree°)			
	Sensor1	Sensor2	Sensor3	Sensor4
CAD Image	-6.8	-51.0	90.5	7.8
Human MRI PCB	-9.5	-53.4	91.1	8.6
Difference of Angle	2.7	2.4	0.6	0.8

Table 8. - Angle of normal vectors in CAD Image and change in normal vectors of middle plane of Human MRI PCB in X-Y, Transverse Plane

CHAPTER IV

DISCUSSION & CONCLUSION

4.1. DISCUSSION

The ultimate goal of this study was to create a valid method for determining IMG PCB sensor position and orientation and to quantify the inaccuracy of this method. The method was combined under two parts. The first part of the study (Validation Part 1) showed that the method used in was accurate enough to calculate position and orientation of "IMG PCB" sensors. In Validation Part 1, the maximum difference in position was **0.46mm** and maximum difference in orientation was **2.1°**. The same method was then applied to the "Human MRI PCB" in Validation Part 2 and the results were very promising. In Validation Part 2, it was observed that the "MRI PCB" positions and orientations in the human mouth calculated a Frankfurt-maxillary angle of **6.8°** versus 10° from literature[22]. The "Human MRI PCB" also had adequate signal-noise ratio which allowed for full usage of the validated method developed in Validation Part 1.In the case of lower quality images, determining a polynomial fit for the MRI PCB

may be employed to identify sensor positions and orientations. This supplemental method is provided in **Appendix B.**

4.2. CONCLUSION

Head injury is a major problem for professional sports players. In this study, position and orientation of IMG sensors were determined to within **0.46 mm** maximum difference in position and **2.1°** difference as an angle for orientation. Based on these promising position and orientation results, it may be possible for the IMG to help fill this gap in the future by measuring head impacts with known error. Based upon the data developed in Validation Parts 1 and 2, the method used in this project appears to be an accurate means to find position and orientation of IMG sensors regardless of sensor position, sensor number, or miniature sensor size. Based on the findings from this study, if an athlete were to receive an impact which effects the CG as linear acceleration magnitude of 132.7g in the X-direction, the CG linear acceleration varies by -0.6g to +0.9gdue to IMG position and orientation inaccuracies. When bounding a 5% error error rate on position and orientation, there must be a 14.8° difference in orientation or 15mm difference in position. The method developed here is simple but reliable and efficient and is deployed using Matlab.

Future work should involve further validation testing using more human scans and correlating external anthropometric landmarks with sensor positions determined by MRI, also evaluating influence of noise on MRI data (**Appendix B**).

REFERENCES

1. Martin, P. G., Crandall, J. R., Pilkey, W. D., Chou, C. C., Fileta, B. B. Measurement Techniques for Angular Velocity and Acceleration in an Impact Environment. SAE 970575, Proceedings of the SAE International Congress & Exposition (SAE SP 1264), Detroit Michigan (1997).

2. Thomas, A. et al. Diffuse Axonal Injury and Traumatic Coma. Annals of Neurosurgery, 12(6):564-574 (2004).

3. Pfister, B. J., Chickola, L., Smith, D. H. Head Motions While Riding Roller Coasters: Implications for Brain Injury. Am. J. Forensic Med. Pathol., 30(4):339-345 (2009).

4. Fuller, C., Junge, A., Dvorak, J. A Six-Year Prospective Study of the Incidence, Etiology and Causes of Head and Neck Injuries in International Football. Br. J. Sports Med. (2005).

5. Annex I - Test Protocol for Occupant Safety Measurements and Injury Assessment. North Atlantic Treaty Organization, Research and Technology Organization (2006).

6. Society of Automative Engineers (SAE). Instrumentation for Impact Tests – Part I – Electronic Instrumentation. SAE J211; Warrendale, PA (1995).

7. G. Roush, Finding Cadaveric Human Head Masses And Center Of Gravity: A Comparison of Direct Measurement To 3d Modeling, Wright State University,(2010)

8. Alzheimer's Disease Neuroimaging Initiative 3T MRI Technical Procedures Manual, Ver.1, (01.31.2011).

9. Analog Devices, High Performance Wide Bandwidth Accelerometer Datasheet, Rev A, (2010)

10. STMicroelectronics, Micro LG4200 datasheet, Rev 2, February (2013)

11. Chandler, R. F, Clauser, C. E, McConville, J. T,Reynolds, H. M, Young, J. W. Investigation of Inertial Properties of the Human Body, March (1975)

12. Gregory G. Slabaugh, Computing Euler angles from a rotation matrix, Clinical Biomechanics, (2005).

13. Andrew R. Kardunaa, Phil W. McClureb, Lori A. Michenerc, Scapular kinematics: effects of altering the Euler angle sequence of rotations, Volume 33, Issue 9, September 2000, Pages 1063–1068

14. P.H. Abrahams, R.T. Hutchings, S.C. Marks Jr, McMINN's Color Atlas of Human Anatomy, 4th Edition, Wolfe Publishing (1998)

15. Goldstein, Herbert, Classical Mechanics (2nd ed.), Reading, MA: Addison Wesley (1980)

16. Newman, J. A., Beusenberg, M. C., Shewchenko, N., Withnall, C., Fournier, E. Verification of Biomechanical Methods Employed in a Comprehensive Study of Mild Traumatic Brain Injury and the Effectiveness of American Football Helmets. Journal of Biomechanics 38:1469-1481 (2005).

17. Martin, P. G., Hall, G. W., Crandall, J. R., Pilkey, W. D. Measuring the Acceleration of A Rigid Body. Engineering and Technology Volume 5, No: 4(1998).

18. Ascher Friedman, Nabil Hajj Chehade, Chieh Chien, Greg Pottie, Estimation of Accelerometer Orientation for Activity Recognition, 34th Annual International Conference of the IEEE EMBS San Diego, California USA, 28 August - 1 September, 2012

19. J. M. McCarthy, "An Introduction to Theoretical Kinematics." MIT Press, 1990.

20. Chételat, G., Baron, J.C., Early diagnosis of Alzheimer's disease: contribution of structural neuroimaging, Neuroimage, 2003.

21. Mansfield, P. (1988) Imaging by Nuclear Magnetic Resonance. J. Phys. E: Sci. Instrum.21,18-30.

22. DiPietro, G.J., Moergeli, J.R., 1976. Significance of the Frankfurt Mandibular Plane Angle to Prosthedontics. J Prosthet Dent., 36(6), 624-635.

23. V. Hasija, E. G. Takhounts, and R. H. Eppinger, Finding 3D Angular Accelerations of a Rigid Body from In-plane Accelerometers Using Optimization, Injury Biomechanics Research, Proceedings of the Thirty-Second International Workshop

APPENDIX

APPENDIX A

FULLCURE 705 MATERIAL DATASHEET

Section 1 - Chemical Product and Company Identification

Product Use: Ink Cartridge - Professional Use

Chemical Name: Ink Cartridge - Professional Use

Manufacturer Information : Billerica, MA 01821 □ +1 978 495 5580 - USA – Multi-lingual response

Section 2 - Hazards Identification

A) Emergency Overview

This product is considered to be an article according to 29 CFR 1910.1200 (OSHA Hazard Communication Standard). While no specific safety information is required for articles, this Material Safety Data Sheet is provided for informational purposes.As manufactured and supplied, the Objet toner cartridge is not hazardous under normal conditions of use. While unlikely, uncured resin may leak from damaged toner cartridges and cause eye and/or skin irritation.

B) Potential Health Effects: Eyes

Uncured resin is expected to be irritating to the eyes. Uncured resin may polymerize and adhere to eye tissue.

C) Potential Health Effects: Skin

Uncured resin is irritating to the skin. Uncured resin may polymerize and adhere to skin. Uncured resin may cause an allergic response in sensitized individuals.

D) Potential Health Effects: Ingestion

Ingestion is not a likely exposure route. Uncured resin is expected to be irritating to the digestive tract. Ingestion of large quantities is likely to cause nausea, vomiting and headache.

E) Potential Health Effects: Inhalation

Inhalation is not a likely exposure route. Inhalation expected to cause respiratory tract irritation and headache.

HMIS Ratings: Health: 1 Fire: 1 Physical Hazard: 0

Hazard Scale: 0 = Minimal 1 = Slight 2 = Moderate 3 = Serious 4 = Severe * = Chronic hazard

Section 3 - Composition / Information on Ingredients

- Component/ Percent
- 1,2-Propylene glycol / %20-50
- Polyethylene glycol / %20-50
- Acrylic monomer / %20-40
- Glycerin / %10-30

- Photoinitiator / %<1

Section 4 - Physical & Chemical Properties

- Appearance: Toner cartridge
- Physical State: article
- pH: NA
- Vapor Pressure: NA
- Vapor Density: NA
- Boiling Point: NA
- Melting Point: NA
- Solubility (H2O): soluble Specific Gravity: NA
- Evaporation Rate: NA Octanol/H2O
- Flash Point: 128 °C Flammability Class: IIIB Combustible Liquid

APPENDIX B

LOW QUALITY MRI IMAGES

For low quality MRI images, determining a polyfit curve to the contour of the MRI PCB might be useful in lieu of attempting to use the GUI developed in Validation Parts 1 and 2. As a first step, a polynomial fit using two methods were created. The degree of polynomial fit was decided based on the R squared correlation of each polynomial fit to the MRI data.

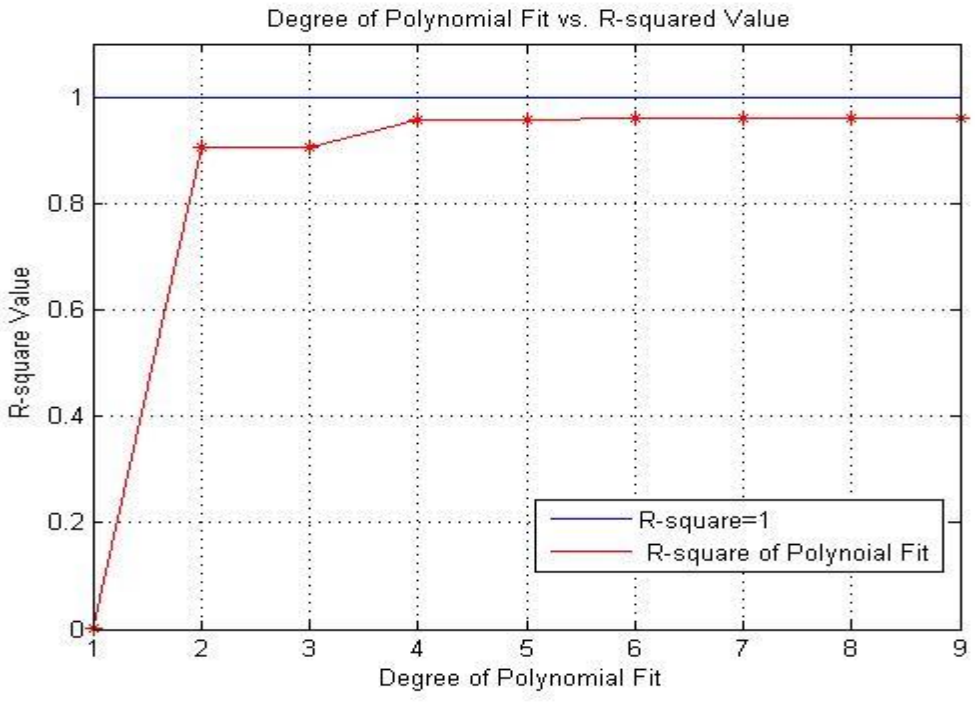

Figure 49. - Degree of Polynomial Fit vs. R-squared Value

Order Number of Polynomial Fit	R-Squared Value	RMS Value
2	0.90	3.8
3	0.90	3.8
4	0.95	2.6
5	0.95	2.6
6	0.95	2.5
7	0.96	2.5
8	0.96	2.5
9	0.96	2.5

Table 9. - R- Squared and RMS Value by order number of Polynomial Fit

At the end of this study, it was decided to select 6th as an order of polynomial fit based on the R-squared values and because the IMG PCB curvature resembles an even ordered polynomial. The 6th order polynomial fit was then applied to the high quality MRI Images and well as the CAD Image.Top view of CAD Image was used to obtain the polynomial equation.

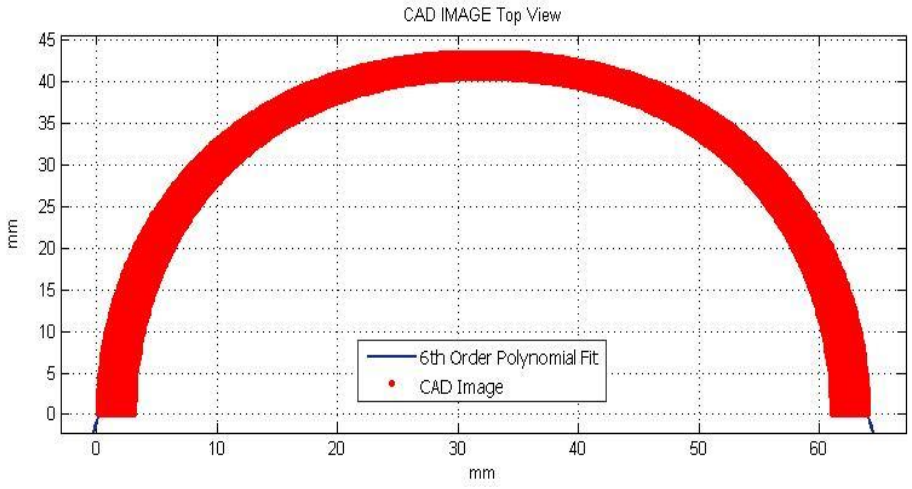

Figure 50. - CAD Image Top View

The equation of the 6th order polynomial fit for the CAD Image is written below Equation (1):

$$(1)\ f(x) = -1.498 * x^6 + 0.009 * x^5 - 4.352 * x^4 + 0.028 * x^3 - 6.643 * x^2 + 0.014 * x^1 + 41.67$$

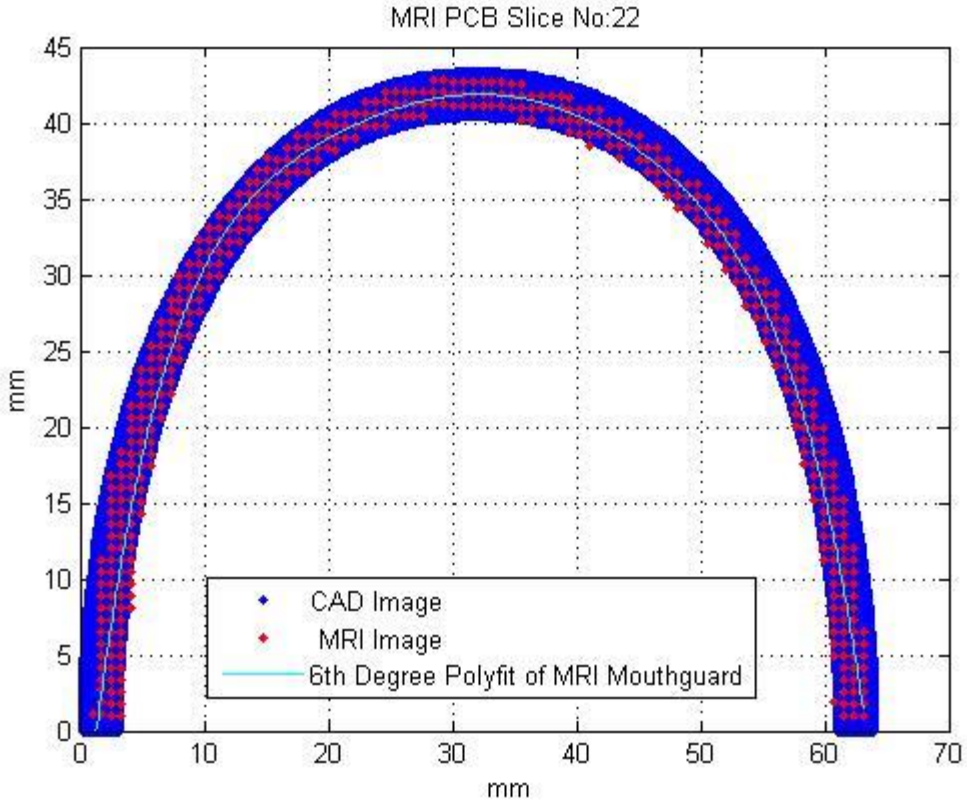

Figure 51. - MRI PCB Slice No:22

The equation of the resulting 6th order polynomial fit for MRI PCB Slice No: 22 is written below in Equation (2):

$$(2)\ f(x) = -6.876 * x^6 + 3.443 * x^5 + 4.025 * x^4 - 2.984 * x^3 - 12.49 * x^2 + 1.247 * x^1 + 41.51$$

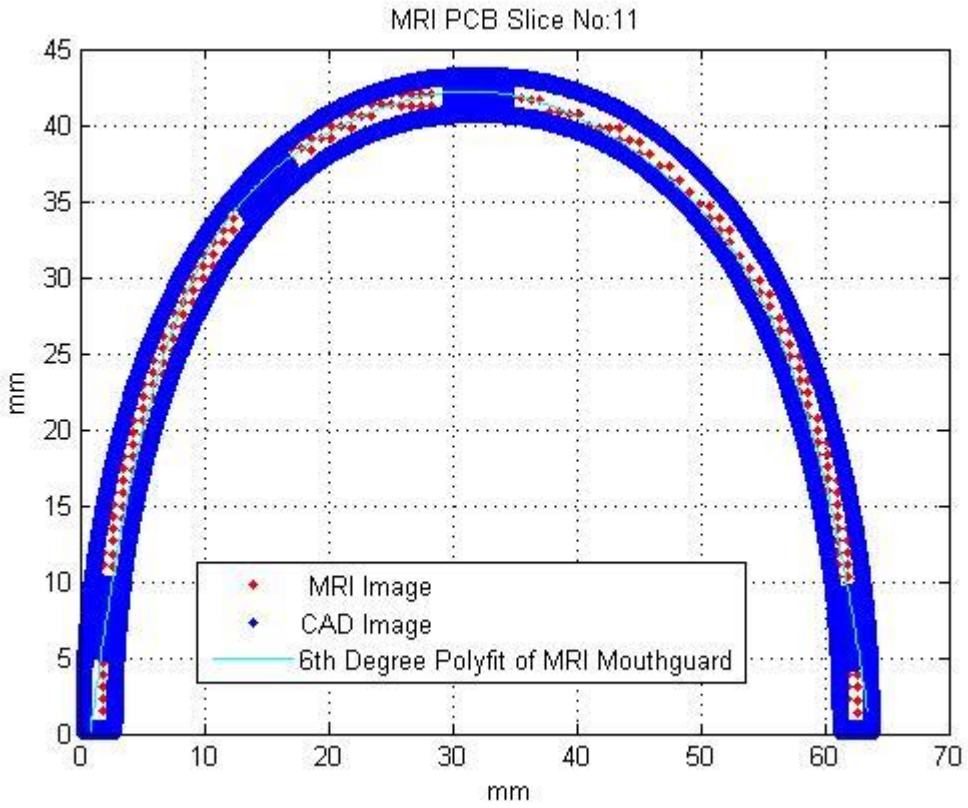

Figure 52. - MRI PCB Slice No:11

The equation of the 6th order polynomial fit for MRI PCB Slice No: 11 is written below (Eq. 3):

$$(3)\ f(x) = -7.731 * x^6 + 5.501 * x^5 + 4.595 * x^4 - 3.406 * x^3 - 13.34 * x^2 + 1.751 * x^1 + 42.17$$

APPENDIX C

I. Head cg anatomical location summary[1]: Author	Year	#Heads	Status	Head CG Location	Age	Head Weight[2] (g)
AVERAGE	**From Roush (2010), Beier (1979), Chandler (1975), Walker (1973)**	53 (51 males, 2 females)	4 fresh 49 embalmed	2.6±0.7 cm superior 0.7±0.6 cm anterior to tragion	55±16	4272±489
Mertz	**1967**	2	Embalmed	5.3cm superior and 2.1cm anterior to occipital condyles	68	3492
Clauser	**1969**	13	Embalmed – with C12 tissue	11.2±0.2cm inferior vertex 8.0±0.2 cm anterior to occiput [47% from vertex, 40% from occiput]	49±14	4729±324
Becker	**1972**	6 male	Embalmed	2.5±1.1cm superior 1.3±0.3cm anterior to tragion[5]	Unknown	3883±471
Walker	**1973**	20 male	Embalmed	2.1±0.5cm superior 0.9±0.7cm anterior to tragion[5]	62±10	4375±591

1) Refers to one standard deviation
2) Hybrid III 50th weight = 4540g (from Backaitis & Mertz, 1994 study on embalmed heads)
3) Used photographic and x-ray methods
4) These specimens included in Walker (1973) dataset
5) Assumes described location (“auditory meatus”) is referencing tragion.
6) Used photographic and x-ray methods

APPENDIX D

TECHNICAL DRAWING OF MRI PCB